

# $\alpha$ -Synuclein strains target distinct brain regions and cell types

Angus Lau<sup>1,2,16</sup>, Raphaella W. L. So<sup>1,2,16</sup>, Heather H. C. Lau<sup>1,2</sup>, Jason C. Sang<sup>3</sup>, Alejandro Ruiz-Riquelme<sup>1,15</sup>, Shelaine C. Fleck<sup>4,5</sup>, Erica Stuart<sup>1</sup>, Sindhu Menon<sup>1</sup>, Naomi P. Visanji<sup>6,7</sup>, Georg Meisl<sup>3</sup>, Rania Faidi<sup>1</sup>, Maria M. Marano<sup>1,8</sup>, Cian Schmitt-Ulms<sup>1</sup>, Zhilan Wang<sup>1</sup>, Paul E. Fraser<sup>1,9</sup>, Anurag Tandon<sup>1,8</sup>, Bradley T. Hyman<sup>10,11,12</sup>, Holger Wille<sup>4,5</sup>, Martin Ingelsson<sup>13</sup>, David Klenerman<sup>3,14</sup> and Joel C. Watts<sup>1,2\*</sup>

**The clinical and pathological differences between synucleinopathies such as Parkinson's disease and multiple system atrophy have been postulated to stem from unique strains of  $\alpha$ -synuclein aggregates, akin to what occurs in prion diseases. Here we demonstrate that inoculation of transgenic mice with different strains of recombinant or brain-derived  $\alpha$ -synuclein aggregates produces clinically and pathologically distinct diseases. Strain-specific differences were observed in the signs of neurological illness, time to disease onset, morphology of cerebral  $\alpha$ -synuclein deposits and the conformational properties of the induced aggregates. Moreover, different strains targeted distinct cellular populations and cell types within the brain, recapitulating the selective targeting observed among human synucleinopathies. Strain-specific clinical, pathological and biochemical differences were faithfully maintained after serial passaging, which implies that  $\alpha$ -synuclein propagates via prion-like conformational templating. Thus, pathogenic  $\alpha$ -synuclein exhibits key hallmarks of prion strains, which provides evidence that disease heterogeneity among the synucleinopathies is caused by distinct  $\alpha$ -synuclein strains.**

Parkinson's disease (PD) and related diseases, including dementia with Lewy bodies (DLB) and multiple system atrophy (MSA), are progressive neurodegenerative disorders. The brains of patients with PD, DLB or MSA contain intracellular inclusions composed of aggregated  $\alpha$ -synuclein. Thus, these diseases are commonly referred to as  $\alpha$ -synucleinopathies or simply synucleinopathies<sup>1</sup>.  $\alpha$ -Synuclein is a 140-amino-acid cytoplasmic protein that is found within presynaptic nerve terminals and is involved in the assembly of SNARE complexes<sup>2</sup>. In disease,  $\alpha$ -synuclein polymerizes into insoluble  $\beta$ -sheet-rich protein aggregates that become phosphorylated at residue Ser 129 and deposit within the CNS<sup>3,4</sup>.  $\alpha$ -Synuclein is believed to play a central pathogenic role in the synucleinopathies, since mutations in the gene encoding  $\alpha$ -synuclein cause early-onset PD or DLB<sup>5</sup>.

There is mounting evidence to indicate that  $\alpha$ -synuclein becomes prion-like during disease, leading to a progressive cell-to-cell spreading of protein aggregates within the brain<sup>6</sup>. Prions are self-propagating protein aggregates that cause neurodegenerative disorders such as Creutzfeldt–Jakob disease in humans and scrapie in sheep. Prion replication and spreading is thought to occur via a template-directed refolding mechanism, in which aggregated prion protein (PrP) catalyzes the conformational conversion of properly folded PrP into additional copies of the misfolded form<sup>7</sup>. Similar to the experimental

transmission of prion disease, injection of mice with preformed  $\alpha$ -synuclein aggregates induces the aggregation and deposition of  $\alpha$ -synuclein within the brain and, in some instances, accelerates the onset of neurological illness<sup>8–13</sup>. The prion-like behavior of  $\alpha$ -synuclein aggregates provides a potential molecular explanation for the progressive nature of PD and related synucleinopathies.

The synucleinopathies are clinically and pathologically heterogeneous, with prominent disease-specific differences in clinical presentation and rate of disease progression, as well as the brain regions and cell types vulnerable to  $\alpha$ -synuclein deposition and cellular death<sup>14,15</sup>. Different types of cerebral  $\alpha$ -synuclein inclusions are observed among the synucleinopathies. For example, the pathological hallmark of PD and DLB is the presence of Lewy bodies (LBs) and Lewy neurites within neurons, whereas MSA is characterized by cytoplasmic  $\alpha$ -synuclein inclusions within oligodendrocytes. One potential explanation for this phenotypic diversity is the presence of different strains of  $\alpha$ -synuclein aggregates, similar to what occurs in prion diseases. Prion strains are different types of prions that possess distinct biochemical and pathological properties<sup>16</sup>. Strain-specific attributes are encoded by unique conformational states of PrP aggregates<sup>17</sup>. Prion strains can be differentiated by their incubation periods following inoculation into animals and the resultant clinical signs of neurological illness, by the location

<sup>1</sup>Tanz Centre for Research in Neurodegenerative Diseases, University of Toronto, Toronto, Ontario, Canada. <sup>2</sup>Department of Biochemistry, University of Toronto, Toronto, Ontario, Canada. <sup>3</sup>Department of Chemistry, University of Cambridge, Cambridge, UK. <sup>4</sup>Centre for Prions and Protein Folding Diseases, University of Alberta, Edmonton, Alberta, Canada. <sup>5</sup>Department of Biochemistry, University of Alberta, Edmonton, Alberta, Canada. <sup>6</sup>Morton and Gloria Shulman Movement Disorders Centre, Toronto Western Hospital, Toronto, Ontario, Canada. <sup>7</sup>Edmond J. Safra Program in Parkinson's Disease, Toronto Western Hospital, Toronto, Ontario, Canada. <sup>8</sup>Department of Medicine, University of Toronto, Toronto, Ontario, Canada. <sup>9</sup>Department of Medical Biophysics, University of Toronto, Toronto, Ontario, Canada. <sup>10</sup>Department of Neurology, Massachusetts General Hospital, Charlestown, MA, USA. <sup>11</sup>Department of Radiology, Massachusetts General Hospital, Charlestown, MA, USA. <sup>12</sup>Neuroscience Program, Harvard Medical School, Boston, MA, USA. <sup>13</sup>Department of Public Health and Caring Sciences/Geriatrics, Uppsala University, Uppsala, Sweden. <sup>14</sup>UK Dementia Research Institute, University of Cambridge, Cambridge, UK. <sup>15</sup>Present address: German Center for Neurodegenerative Diseases (DZNE), Tübingen, Germany. <sup>16</sup>These authors contributed equally: Angus Lau, Raphaella W. L. So. \*e-mail: [joel.watts@utoronto.ca](mailto:joel.watts@utoronto.ca)

and morphology of prion aggregates within the brain and by their conformational properties. A key feature of prion strains is that their biological properties are maintained after serial transmission due to template-directed misfolding.

Several recent studies have provided evidence that  $\alpha$ -synuclein can exhibit strain-like behavior in vitro and following inoculation into rodents. For instance, recombinant  $\alpha$ -synuclein can be polymerized into distinct aggregated states that exhibit differential toxicities when applied to cultured cells, demonstrate distinct abilities to promote tau inclusions in neurons and display variable capacities to spread and induce pathology when injected into rodents<sup>18–20</sup>. Furthermore, different synucleinopathy samples exhibit distinct seeding capacities in vitro and in vivo, with MSA-derived  $\alpha$ -synuclein aggregates being more potent inducers of  $\alpha$ -synuclein pathology than PD-derived aggregates<sup>21–24</sup>. MSA brain extracts can also induce distinct  $\alpha$ -synuclein pathologies when injected into different lines of transgenic mice<sup>25</sup>. While these results are consistent with the existence of  $\alpha$ -synuclein strains, whether distinct conformational states of  $\alpha$ -synuclein aggregates exhibit all the salient properties of prion strains when propagated in animals, including the ability to initiate truly distinct, serially transmissible synucleinopathies in the same host, remains unknown.

Here, we demonstrate that different strains of recombinant or brain-derived  $\alpha$ -synuclein aggregates produce unique motor, pathological and biochemical phenotypes after propagation in TgM83 transgenic mice. Most notably, different  $\alpha$ -synuclein strains target distinct brain regions and cell types within the inoculated mice, thereby recapitulating the selective targeting observed between different human synucleinopathies. Strain-specific phenotypic differences are maintained after serial transmission, which indicates that  $\alpha$ -synuclein aggregate strains propagate via a prion-like templating mechanism and thus behave similarly to prion strains.

## Results

**Generation of recombinant  $\alpha$ -synuclein fibril strains.** We hypothesized that unique conformational states of  $\alpha$ -synuclein aggregates ( $\alpha$ -synuclein strains) would produce distinct phenotypes when propagated in the TgM83 synucleinopathy mouse model, which overexpresses  $\alpha$ -synuclein containing the disease-causing A53T mutation<sup>26</sup>. Based on the published success of generating distinct recombinant  $\alpha$ -synuclein strains by varying buffer conditions during fibril formation<sup>19,20</sup>, we initially searched for conditions that produced A53T-mutant human  $\alpha$ -synuclein fibrils with divergent conformational properties. We focused on fibrils since they appear to be more potent inducers of PD-like neuropathology than  $\alpha$ -synuclein oligomers after injection into mice<sup>20,27</sup>. Polymerization of recombinant  $\alpha$ -synuclein in either the presence or absence of 100 mM NaCl generated conformationally distinct aggregates, which we termed salt (S) and no salt (NS) fibrils (Fig. 1a). In real-time thioflavin T (ThT) fluorescence aggregation assays, the lag phase for S fibril formation was significantly shorter than for NS fibrils (Fig. 1b). Interestingly, NS fibrils consistently bound much less ThT than S fibrils, which possibly indicates structural differences between the two types of fibrils (Fig. 1c). Indeed, NS fibrils were significantly longer than S fibrils (Fig. 1d), and distinct banding patterns were obtained following digestion of the two fibril types with proteinase K (PK) (Fig. 1e). Moreover, the fluorescence emission spectra obtained following binding of the conformation-sensitive dye curcumin<sup>28</sup> to S and NS fibrils were markedly different (Fig. 1f; Extended Data Fig. 1). Finally, using a conformational stability assay (CSA) that measures the differential abilities of protein aggregate strains to resist denaturation by guanidine hydrochloride (GdnHCl), we found that S fibrils were significantly less stable than NS fibrils (Fig. 1g,h). Taken together, these results demonstrate that the S and NS fibril preparations contain conformationally distinct species of  $\alpha$ -synuclein aggregates.

Next, we assessed whether S and NS fibrils can seed the formation of distinct  $\alpha$ -synuclein aggregates in cultured cells. Using liposome-mediated transduction, various forms of  $\alpha$ -synuclein were introduced into HEK293 cells that stably express human A53T-mutant  $\alpha$ -synuclein fused at its carboxyl terminus with yellow fluorescent protein (YFP)<sup>29</sup> (Extended Data Fig. 2). When cells were treated with monomeric (nonpolymerized) recombinant A53T-mutant  $\alpha$ -synuclein, only diffuse cytoplasmic fluorescence was observed. In contrast, the transduction of either S or NS fibrils resulted in the production of fluorescent foci, which are indicative of the formation of  $\alpha$ -synuclein(A53T)-YFP aggregates. The morphologies of the resultant aggregates differed between the fibril strains, whereby cells exposed to S fibrils developed globular aggregates and cells treated with NS fibrils developed thread-like aggregates (Extended Data Fig. 2).

**Propagation of  $\alpha$ -synuclein strains in TgM83 mice.** When injected into mice, prion strains produce distinct disease phenotypes that are faithfully maintained over serial passaging. To assess whether the same is true of  $\alpha$ -synuclein strains in vivo, we performed propagation studies in hemizygous TgM83 mice (Fig. 2a), which can develop a synucleinopathy following inoculation with preformed  $\alpha$ -synuclein aggregate seeds<sup>9,10</sup>. Hemizygous TgM83 mice were used since they remain healthy for up to at least 20 months of age<sup>10</sup> (Table 1), whereas homozygous mice (M83<sup>+/+</sup>) develop spontaneous signs of neurological illness beginning at around 8 months of age<sup>26</sup>. To determine whether disease phenotypes can be faithfully maintained over multiple passages, brain extracts from previously inoculated mice were used as inocula for serial transmission experiments (Fig. 2a).

Equal amounts (1  $\mu$ g) of S and NS fibril preparations were intracerebrally inoculated into weanling TgM83 mice. As negative controls, we injected mice with either phosphate-buffered saline (PBS) or nonpolymerized monomeric A53T-mutant  $\alpha$ -synuclein. None of the control-inoculated mice developed signs of neurological illness for up to 18 months post-inoculation (Table 1; Fig. 2b). While both groups of fibril-injected animals developed signs of neurological illness that was consistent with a synucleinopathy, the disease incubation periods were markedly different. Mice injected with NS fibrils took longer to develop disease than mice injected with S fibrils, and the distinct disease kinetics were maintained over serial passaging (Table 1; Fig. 2b,c). Strikingly, the clinical signs of neurological illness differed in the fibril-inoculated mice (Supplementary Videos 1–6). Mice injected with S fibrils presented with partial or complete hindlimb paralysis accompanied by bradykinesia, whereas NS fibril-injected mice presented with weight loss, mild kyphosis and a unique hindlimb shaking phenotype. The divergent clinical profiles were maintained following second and third passage of the S-fibril-derived and NS-fibril-derived strains.

To search for a molecular explanation for the incubation period differences, we employed a single-molecule fluorescence approach to study the relative multiplication rates of S and NS fibrils. In this assay, monomeric A53T-mutant  $\alpha$ -synuclein was seeded with either S or NS fibrils, and then fibril length was measured as a function of time by ThT staining and total internal reflection fluorescence microscopy (TIRF)<sup>30</sup>. Using this approach, the time taken for the number of aggregates to double was calculated as a function of the rate constants for fibril elongation and fragmentation (Extended Data Fig. 3). In accordance with the in vivo propagation results, these experiments indicated that NS fibrils exhibited an increased doubling time compared with S fibrils, which can be attributed almost exclusively to their decreased rate of fragmentation (Extended Data Fig. 3; Supplementary Table 1).

To determine whether strain-like behavior also occurs with  $\alpha$ -synuclein aggregates generated in a more physiological environment, we performed transmission studies in TgM83 mice with

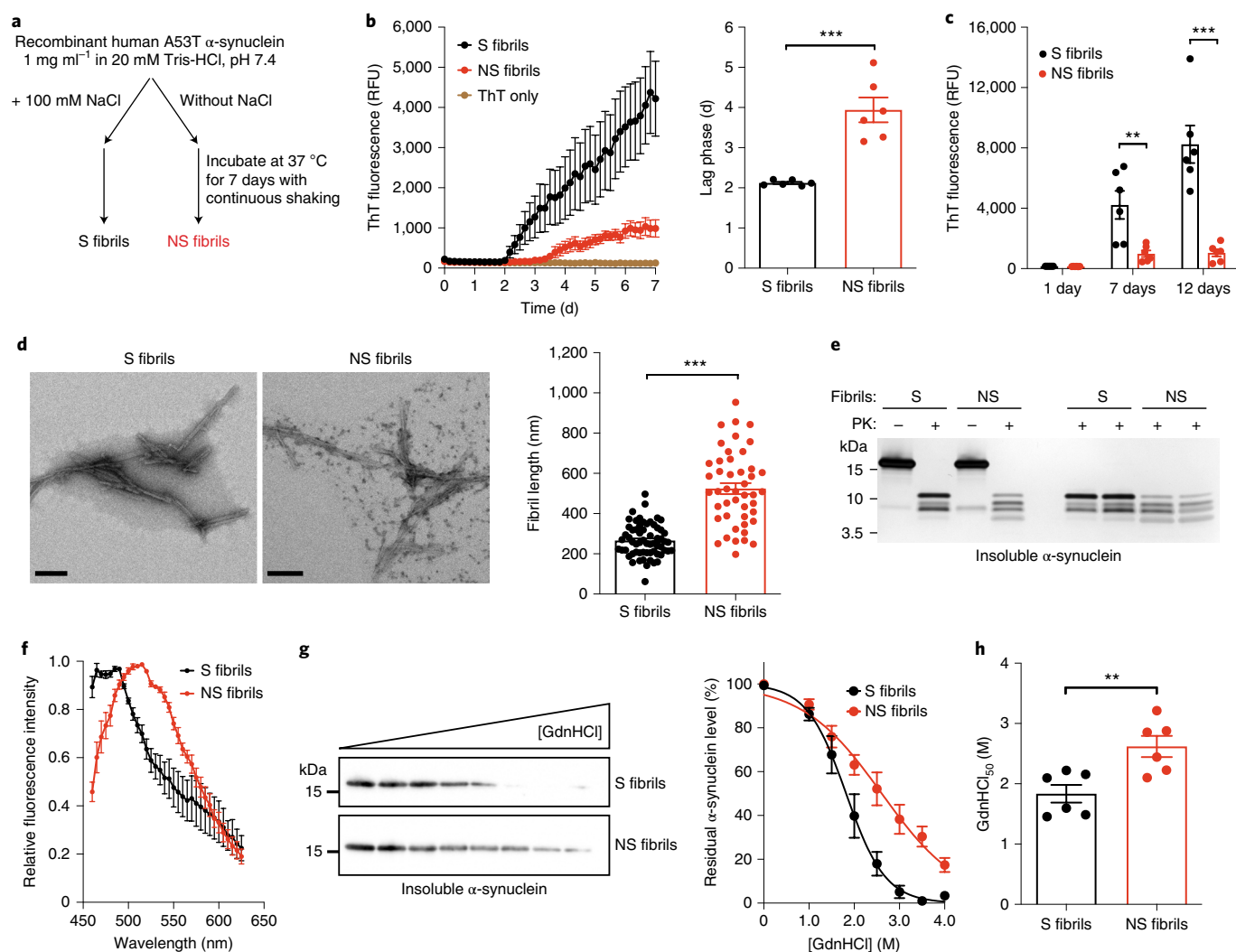


**Fig. 1 | Generation and characterization of recombinant  $\alpha$ -synuclein fibril strains.** **a**, Schematic of the conditions used for generating S and NS fibrils. **b**, Left: kinetics of fibril formation for S and NS fibrils in a real-time ThT fluorescence assay. Reactions containing only ThT were used as a negative control. Right: the lag phase for S fibril formation was significantly shorter than the lag phase for NS fibril formation ( $***P=1.6 \times 10^{-4}$  by a two-tailed  $t$ -test).  $n=6$  biologically independent reactions. RFU, relative fluorescence units. **c**, After 7 or 12 days of incubation, NS fibrils bind significantly less ThT than S fibrils ( $**P=0.0041$  for day 7,  $***P=2.7 \times 10^{-8}$  for day 12 by two-way ANOVA with Sidak's multiple comparison test).  $n=6$  biologically independent reactions. **d**, At the ultrastructural level, NS fibrils are significantly longer than S fibrils, as determined by electron microscopy ( $***P=2.5 \times 10^{-5}$  by a two-tailed  $t$ -test).  $n=3$  biologically independent fibril preparations. Scale bars, 200 nm. **e**, Following digestion with PK, S fibrils and NS fibrils produce different banding patterns of insoluble  $\alpha$ -synuclein species, as assessed by SDS-PAGE followed by silver staining. For both S and NS fibrils, three biologically independent fibril preparations were analyzed. **f**, The fluorescence emission spectra for curcumin bound to S and NS fibrils are distinct. Each data point represents the mean relative fluorescence obtained from three biologically independent fibril preparations  $\pm$  s.e.m. **g**, CSA for S and NS fibrils. Representative  $\alpha$ -synuclein immunoblots (Syn-1 antibody) and the resultant denaturation curves are shown. The curves depict mean residual  $\alpha$ -synuclein values  $\pm$  s.e.m. following treatment with the indicated concentrations of GdnHCl.  $n=6$  biologically independent fibril preparations. **h**, S fibrils are significantly less stable than NS fibrils ( $**P=0.0065$  by a two-tailed  $t$ -test).  $n=6$  biologically independent fibril preparations. For **b**, **c**, **d** and **h**, data represent the mean  $\pm$  s.e.m.

putative brain-derived strains of  $\alpha$ -synuclein aggregates (Fig. 2a). It has previously been shown that brain extracts from patients with MSA and from sick M83<sup>+/+</sup> mice produce distinct disease kinetics when injected into TgM83 mice<sup>10,11</sup>. In agreement with these results, disease incubation periods following inoculation with brain extract from a patient with MSA were significantly shorter than for TgM83 mice inoculated with brain extract from a spontaneously sick M83<sup>+/+</sup> mouse (Table 1; Fig. 2d,e). The incubation period difference was also observed following second passage of the two brain-derived strains. Moreover, the clinical signs of neurological illness were distinct in MSA-inoculated and M83<sup>+/+</sup>-inoculated TgM83 mice and were maintained following second passage. Hindlimb paralysis and bradykinesia predominated in

MSA-challenged mice, similar to the phenotype observed in mice inoculated with S fibrils, whereas hindlimb shaking, weight loss and mild kyphosis were observed in M83<sup>+/+</sup>-inoculated mice, similar to the phenotype induced by inoculation with NS fibrils (Supplementary Videos 7 and 8).

Detergent-insoluble  $\alpha$ -synuclein species were detected in brain homogenates from all mice examined, including asymptomatic buffer-inoculated animals (Fig. 2f), which is likely due to the overexpression of mutant  $\alpha$ -synuclein in the TgM83 line. However, only the brains of mice injected with  $\alpha$ -synuclein fibrils, M83<sup>+/+</sup> extract or MSA extract contained detergent-insoluble  $\alpha$ -synuclein species that were partially resistant to digestion with the protease thermolysin. Moreover, insoluble  $\alpha$ -synuclein phosphorylated

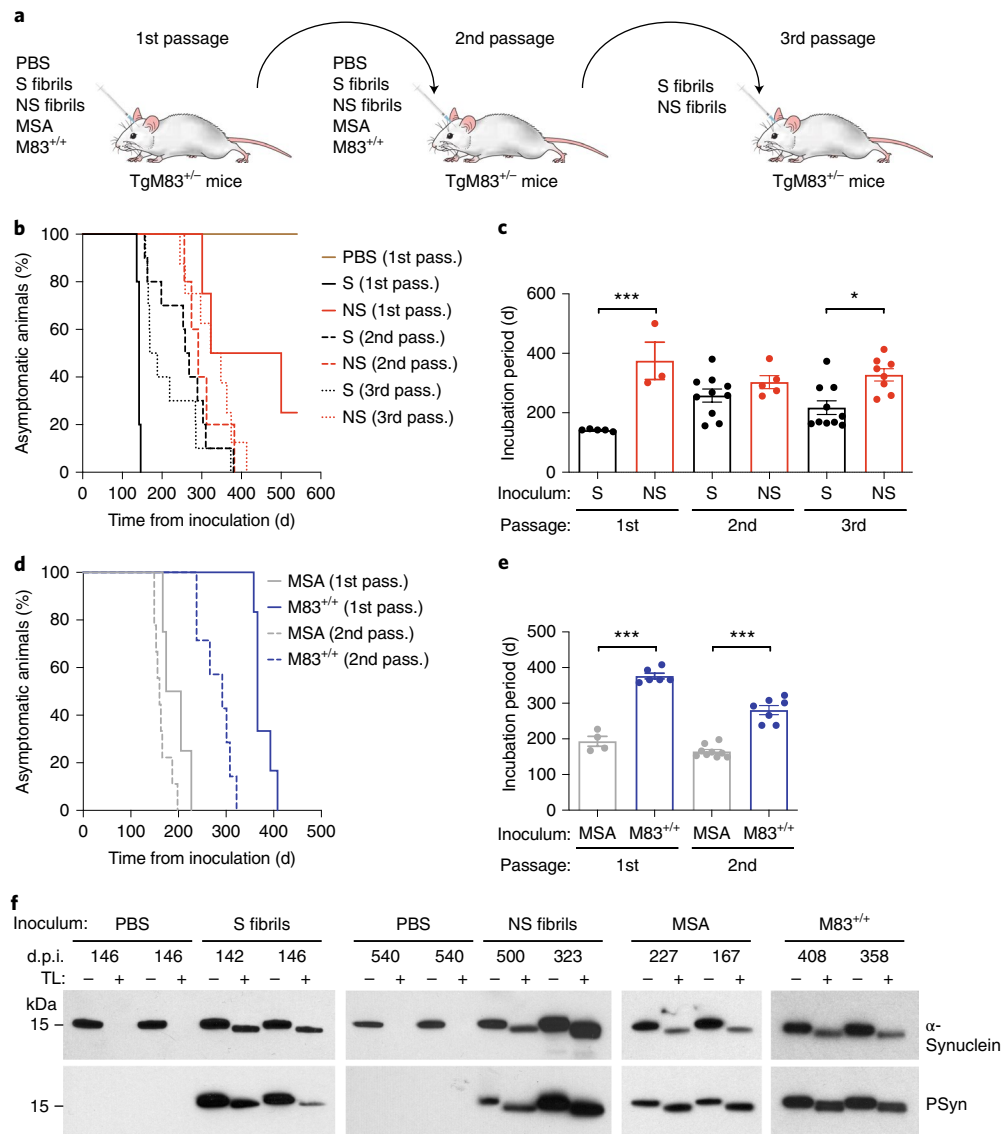


**Fig. 2 | Serial propagation of recombinant and brain-derived  $\alpha$ -synuclein strains in TgM83 mice.** **a**, Schematic of the serial propagation studies in hemizygous TgM83 mice (TgM83<sup>+/-</sup>). **b**, Kaplan-Meier survival curves for TgM83 mice inoculated with PBS, S fibrils or NS fibrils (first, second or third passage (pass.)).  $n = 7$  (PBS), 5 (S, first passage), 4 (NS, first passage), 10 (S, second passage), 5 (NS, second passage), 10 (S, third passage) or 8 mice (NS, third passage). **c**, Following the first or third passage, the incubation periods for the NS-fibril-derived strain were significantly longer than for the S-fibril-derived strain ( $***P = 3.0 \times 10^{-4}$  for first passage,  $*P = 0.013$  for third passage by one-way ANOVA with Tukey's multiple comparisons test).  $n = 5$  (S, first passage), 3 (NS, first passage), 10 (S, second passage), 5 (NS, second passage), 10 (S, third passage) or 8 mice (NS, third passage). Data represent the mean  $\pm$  s.e.m. **d**, Kaplan-Meier survival curves for TgM83 mice inoculated with either MSA or M83<sup>+/-</sup> brain extract (first or second passage).  $n = 4$  (MSA, first passage), 6 (M83<sup>+/-</sup>, first passage), 9 (MSA, second passage) or 7 mice (M83<sup>+/-</sup>, second passage). **e**, For both the first and second passage, the incubation periods for mice injected with the M83<sup>+/-</sup>-derived strain were significantly longer than for mice injected with the MSA-derived strain ( $***P = 5.6 \times 10^{-10}$  for first passage,  $***P = 2.5 \times 10^{-8}$  for second passage by one-way ANOVA with Tukey's multiple comparisons test).  $n = 4$  (MSA, first passage), 6 (M83<sup>+/-</sup>, first passage), 9 (MSA, second passage) or 7 mice (M83<sup>+/-</sup>, second passage). Data represent the mean  $\pm$  s.e.m. **f**, Immunoblots of detergent-insoluble  $\alpha$ -synuclein species, with or without thermolysin (TL) digestion, in brain homogenates from asymptomatic PBS-inoculated TgM83 mice or clinically ill TgM83 mice at the indicated days post-inoculation (d.p.i.) with the indicated  $\alpha$ -synuclein strains (first passage). Blots were probed with antibodies to either total  $\alpha$ -synuclein or PSyn. For each inoculum, results from two distinct mice are shown.

at Ser129 (PSyn), a marker for disease-associated  $\alpha$ -synuclein species<sup>3</sup>, was only detected in brain extracts from the animals injected with samples containing  $\alpha$ -synuclein aggregates (Fig. 2f). Identical results were obtained with brain samples from the serial transmission of the fibril-derived and brain-extract-derived strains (Extended Data Fig. 4). Since TgM83 mice express both A53T-mutant human  $\alpha$ -synuclein and endogenous murine  $\alpha$ -synuclein, we checked whether the induced  $\alpha$ -synuclein aggregates were composed of human  $\alpha$ -synuclein, mouse  $\alpha$ -synuclein or a mixture of

both. Thermolysin-resistant  $\alpha$ -synuclein species in the inoculated TgM83 mice were detectable using an antibody specific for human  $\alpha$ -synuclein but not with an antibody specific for mouse  $\alpha$ -synuclein, which indicates that aggregates are composed exclusively of human  $\alpha$ -synuclein (Extended Data Fig. 4). Immunohistochemistry experiments showed that PSyn deposits were present in the brains of all TgM83 mice inoculated with  $\alpha$ -synuclein fibrils, M83<sup>+/-</sup> extract or MSA extract, but not in the brains of mice injected with PBS or monomeric  $\alpha$ -synuclein (Extended Data Fig. 5). Together, these

**Table 1 | Disease incubation periods for inoculated TgM83 mice**

| Inoculum                     | $\alpha$ -Synuclein sequence in inoculum | First passage                            |                      | Second passage <sup>a</sup>              |                   | Third passage <sup>a</sup>               |         |
|------------------------------|--|--|----------------------|--|-------------------|--|---------|
|                              |  | Mean incubation time $\pm$ s.e.m. (days) | $n/n_0$ <sup>b</sup> | Mean incubation time $\pm$ s.e.m. (days) | $n/n_0$           | Mean incubation time $\pm$ s.e.m. (days) | $n/n_0$ |
| None                         | NA                                       | >540 <sup>c</sup>                        | 0/13                 | ND                                       | ND                | ND                                       | ND      |
| PBS                          | NA                                       | >540                                     | 0/7                  | >400                                     | 0/9               | ND                                       | ND      |
| $\alpha$ -Synuclein monomers | WT                                       | >362                                     | 0/8                  | ND                                       | ND                | ND                                       | ND      |
|                              | A53T                                     | >541                                     | 0/7                  | ND                                       | ND                | ND                                       | ND      |
| S fibrils                    | A53T                                     | 142 $\pm$ 2                              | 5/5                  | 258 $\pm$ 22                             | 10/10             | 217 $\pm$ 23                             | 10/10   |
| NS fibrils                   | A53T                                     | 375 $\pm$ 63                             | 3/4 <sup>d</sup>     | 303 $\pm$ 22                             | 5/5               | 328 $\pm$ 21                             | 8/8     |
| PMCA fibrils                 | WT                                       | 176 $\pm$ 6                              | 8/8                  | 227 $\pm$ 21                             | 9/10 <sup>e</sup> | ND                                       | ND      |
| M83 <sup>+/+</sup>           | A53T                                     | 376 $\pm$ 8                              | 6/6                  | 281 $\pm$ 13                             | 7/7               | ND                                       | ND      |
| MSA                          | WT                                       | 193 $\pm$ 14                             | 4/4                  | 165 $\pm$ 6                              | 9/9               | ND                                       | ND      |
| DLB                          | WT                                       | >540                                     | 0/5                  | ND                                       | ND                | ND                                       | ND      |
| AD                           | WT                                       | >540                                     | 0/4                  | ND                                       | ND                | ND                                       | ND      |

<sup>a</sup>For the second passage, mice were inoculated with brain homogenate from the first-passage mice previously inoculated with the indicated inoculum; for the third passage, mice were inoculated with brain homogenate from second-passage mice. <sup>b</sup> $n$ , number of mice with neurological dysfunction and cerebral PSyn deposition;  $n_0$ , number of mice observed; does not include mice that died of intercurrent illness (see Supplementary Table 4). <sup>c</sup>Mice were examined up until 580 days of age, which corresponds to ~540 days following mock inoculation. <sup>d</sup>One mouse remained healthy at 540 d.p.i. <sup>e</sup>One mouse remained healthy at 375 d.p.i. NA, not applicable; ND, not determined.

results confirm that TgM83 mice develop a synucleinopathy following injection with various  $\alpha$ -synuclein strains.

**$\alpha$ -Synuclein strains produce distinct synucleinopathies in TgM83 mice.** The distribution of PSyn deposits within the brain differed in mice injected with either S or NS fibrils, and these distinct signatures were maintained after serial passaging (Fig. 3a). Both groups of inoculated mice exhibited prominent PSyn pathology in the midbrain, brainstem and hypothalamus (Fig. 3a; Extended Data Fig. 5). However, only mice injected with NS fibrils displayed PSyn deposition in the hippocampus and olfactory bulb, and NS fibril-injected mice had significantly higher levels of PSyn pathology in the cortex than mice inoculated with S fibrils (Fig. 3a,b). Similar to what was observed in mice injected with fibril-derived strains, the neuroanatomical distributions of PSyn pathology in TgM83 mice injected with MSA or M83<sup>+/+</sup> extract were also distinct and stably maintained following serial passaging (Fig. 3c). Higher levels of cortical PSyn deposition were observed in the M83<sup>+/+</sup>-injected animals, and hippocampal and olfactory bulb PSyn pathology was exclusively present in mice inoculated with M83<sup>+/+</sup> extract (Fig. 3c,d). Extensive PSyn deposition within the midbrain, brainstem and hypothalamus was present in mice injected with either MSA or M83<sup>+/+</sup> extract (Fig. 3c; Extended Data Fig. 5). In general, mice injected with either the NS-fibril-derived or M83<sup>+/+</sup>-derived strains exhibited more widespread deposition of PSyn than mice injected with the S-fibril-derived or MSA-derived strains.

In addition to the region-specific differences in PSyn deposition displayed by the various  $\alpha$ -synuclein strains, the cellular tropism of the aggregates was also distinct. In TgM83 mice injected with S fibrils, PSyn pathology was exclusively observed within neurons (Extended Data Fig. 5). While mice injected with NS fibrils also exhibited neuronal PSyn deposition, PSyn staining was additionally observed within astrocytes (Fig. 4a,b). Astrocytic PSyn pathology was observed across all three passages of the NS-fibril-derived strain. TgM83 mice injected with M83<sup>+/+</sup> extract also displayed PSyn pathology within astrocytes (Fig. 4a,b), whereas the PSyn deposits in MSA-injected mice were only found in neurons (Extended Data Fig. 5). In mice injected with either the NS-fibril-derived or M83<sup>+/+</sup>-derived strains, cellular co-localization was observed between PSyn staining and the astrocyte-specific marker glial fibrillary

acidic protein (GFAP), which confirms that the PSyn deposits were present within astrocytes (Fig. 4c).

In regions of the brain targeted by both the S and NS fibril strains, such as the midbrain and hypothalamus, the morphology of the induced  $\alpha$ -synuclein deposits differed substantially. Ring-like PSyn deposits that filled the entire cell body surrounding the nucleus were found within neurons of mice inoculated with S fibrils (Fig. 5a,b). These inclusions were morphologically similar to the neuronal cytoplasmic inclusions found in the hippocampus of patients with atypical MSA<sup>31</sup>. In contrast, single large and dense LB-like PSyn deposits were found within the cytoplasm of neurons from mice inoculated with NS fibrils (Fig. 5a,b). These distinct aggregate morphologies were also visualized using antibodies specific for total  $\alpha$ -synuclein and p62 (also known as SQSTM1), which indicates that both types of deposits were targeted for autophagy (Extended Data Fig. 6). Mice injected with MSA extract exhibited ring-like PSyn deposits, whereas mice injected with M83<sup>+/+</sup> extract displayed LB-like PSyn deposits, which mirrored the pathological differences in mice injected with S or NS fibrils (Fig. 5a,b). The distinct morphologies of PSyn deposits were maintained following serial passaging in TgM83 mice. Thus, much like prion strains,  $\alpha$ -synuclein strains can target distinct regions and cell types within the brain and induce the formation of aggregates with distinct morphologies.

Biochemical analyses of the  $\alpha$ -synuclein aggregates in the brains of mice inoculated with the various  $\alpha$ -synuclein strains revealed conformational differences. The banding pattern of PK-resistant  $\alpha$ -synuclein species in mice injected with S fibrils was slightly different from that in mice injected with NS fibrils. While both groups of mice possessed a band at ~9kDa, mice injected with S fibrils exhibited an additional band at ~10kDa, whereas mice injected with NS fibrils displayed a prominent additional lower band at ~7kDa (Fig. 5c). The distinct PK digestion signatures were maintained after serial passaging, but only partially overlapped with the pattern generated by digestion of the original fibrils (Extended Data Fig. 7). Similar differences in PK-resistant  $\alpha$ -synuclein banding patterns were observed between MSA-injected and M83<sup>+/+</sup>-injected mice (Fig. 5c). As assessed using the CSA, the aggregates present in S-fibril-injected mice were significantly less stable following exposure to GdnHCl than those in NS-fibril-inoculated animals, and this difference in conformational stability was preserved following

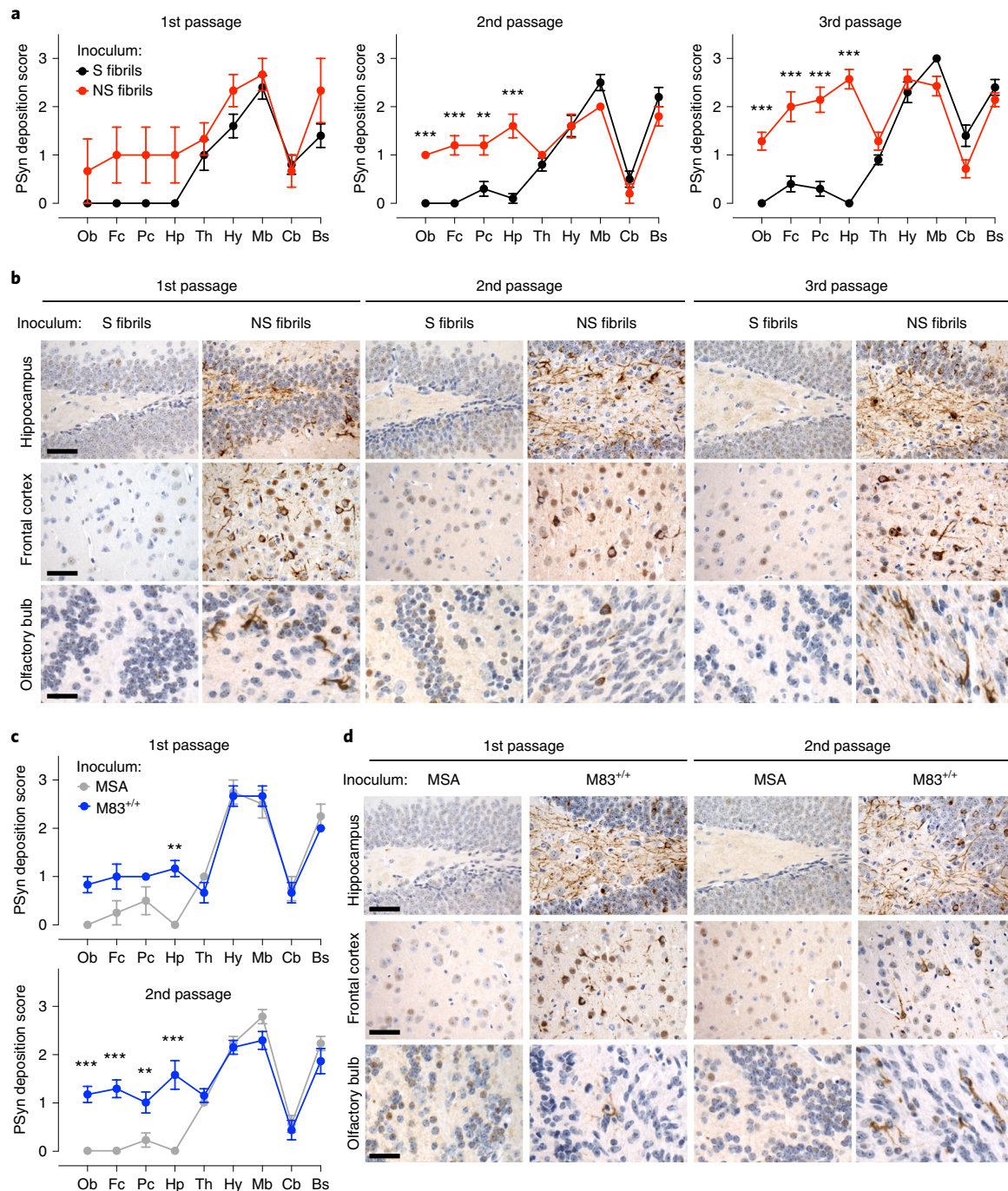


**Fig. 3** |  $\alpha$ -Synuclein strains target distinct brain regions in TgM83 mice. **a**, Semiquantitative PSyn deposition scoring within the indicated brain regions from clinically ill TgM83 mice following the first, second or third passage of the S-fibril-derived or NS-fibril-derived strains. The patterns of PSyn deposition were significantly different for the S-fibril-derived and NS-fibril-derived strains following the second ( $P=0.012$ ) and third passage ( $P=6.5 \times 10^{-5}$ ), as determined by two-way ANOVA.  $n=5$  (S, first passage), 3 (NS, first passage), 10 (S, second passage), 5 (NS, second passage), 10 (S, third passage) or 7 mice (NS, third passage). Data represent the mean  $\pm$  s.e.m.  $^{**}P < 0.01$ ,  $^{***}P < 0.001$  as determined by Sidak's multiple comparisons test. Bs, brainstem; Cb, cerebellar white matter; Fc, frontal cortex; Hp, hippocampus; Hy, hypothalamus; Mb, midbrain; Ob, olfactory bulb; Pc, parietal cortex; Th, thalamus. **b**, Representative immunohistochemistry images of PSyn in the hippocampus (dentate gyrus region), frontal cortex or olfactory bulb from mice following inoculation with the S-fibril-derived or NS-fibril-derived strains (first, second or third passage). **c**, Semiquantitative PSyn deposition scoring within the indicated brain regions from clinically ill TgM83 mice following the first or second passage of the MSA-derived or M83<sup>+/+</sup>-derived strains. The patterns of PSyn deposition were significantly different for the MSA-derived and M83<sup>+/+</sup>-fibril-derived strains after the second passage ( $P=0.0041$ ), as determined by two-way ANOVA.  $n=4$  (MSA, first passage), 6 (M83<sup>+/+</sup>, first passage), 9 (MSA, second passage) or 7 mice (M83<sup>+/+</sup>, second passage). Data represent the mean  $\pm$  s.e.m.  $^{**}P < 0.01$ ,  $^{***}P < 0.001$  as determined by Sidak's multiple comparisons test. **d**, Representative immunohistochemistry for PSyn in the hippocampus (dentate gyrus region), frontal cortex or olfactory bulb from symptomatic mice following inoculation with the MSA-derived or M83<sup>+/+</sup>-derived strains (first or second passage). Scale bars, 50  $\mu$ m (hippocampus and frontal cortex) or 25  $\mu$ m (olfactory bulb) for both **b** and **d**.

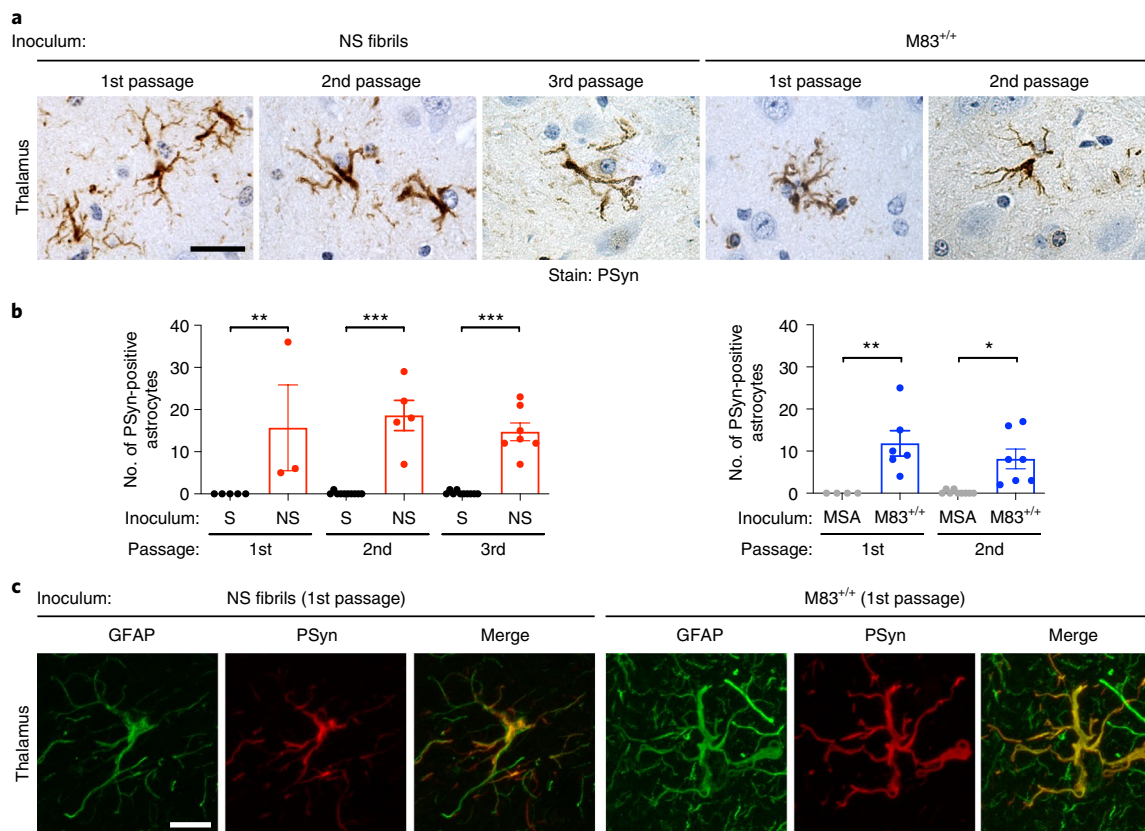


**Fig. 4 | The NS-fibril-derived and M83<sup>+/+</sup>-derived  $\alpha$ -synuclein strains selectively target astrocytes in TgM83 mice.** **a**, Representative immunohistochemistry images of PSyn in the thalamus of clinically ill TgM83 mice inoculated with either the NS-fibril-derived strain (first, second or third passage) or the M83<sup>+/+</sup>-derived strain (first or second passage) reveals  $\alpha$ -synuclein pathology within astrocytes. Scale bar, 25  $\mu$ m (applies to all images). **b**, Quantification of PSyn-positive astrocytes within the thalamus of TgM83 mice inoculated with either the S-fibril-derived or NS-fibril-derived strains (first, second or third passage), as well as TgM83 mice inoculated with either the MSA-derived or M83<sup>+/+</sup>-derived strains (first or second passage). Significantly more PSyn-positive astrocytes were present in mice inoculated with the NS-fibril-derived strain compared with mice inoculated with the S fibril-derived strain (\*\* $P=0.0064$ , \*\*\* $P=1.1 \times 10^{-5}$  and \*\*\* $P=1.1 \times 10^{-4}$  for first, second and third passages, respectively), as well as in mice inoculated with the M83<sup>+/+</sup>-derived strain compared with mice inoculated with the MSA-derived strain (\*\* $P=0.0047$  and \* $P=0.016$  for first and second passages, respectively), as determined by one-way ANOVA with Tukey's multiple comparisons test.  $n=5$  (S, first passage), 3 (NS, first passage), 10 (S, second passage), 5 (NS, second passage), 10 (S, third passage), 7 (NS, third passage), 4 (MSA, first passage), 6 (M83<sup>+/+</sup>, first passage), 9 (MSA, second passage) or 7 mice (M83<sup>+/+</sup>, second passage). Data represent the mean  $\pm$  s.e.m. **c**, Co-localization of PSyn (red) and GFAP (green) staining in double-labeled sections of the thalamus from TgM83 mice inoculated with either NS fibrils or M83<sup>+/+</sup> brain extract (first passage). Scale bar, 10  $\mu$ m (applies to all images).

serial propagation (Fig. 5d,e; Extended Data Fig. 8). Across two passages, the  $\alpha$ -synuclein aggregates in TgM83 mice injected with MSA extract were also more susceptible to GdnHCl denaturation than those in mice inoculated with M83<sup>+/+</sup> extract (Extended Data Fig. 8), a result reminiscent of the differences observed between animals inoculated with the S-fibril-derived or NS-fibril-derived strains.

**Not all recombinant  $\alpha$ -synuclein strains produce distinct synucleinopathies in TgM83 mice.** Having established that the S and NS strains of recombinant  $\alpha$ -synuclein aggregates can produce distinct synucleinopathies, we wondered whether additional strains could be propagated in TgM83 mice. To this end, we generated fibrils from wild-type (WT) or A53T-mutant recombinant human  $\alpha$ -synuclein using either a continuous shaking protocol or by intermittent sonication using protein misfolding cyclic amplification (PMCA). Consistent with previous results<sup>32</sup>, recombinant  $\alpha$ -synuclein aggregated rapidly during the PMCA procedure and produced very short fibrils (Fig. 6a; Extended Data Fig. 9). Following PK digestion, we found that the PMCA fibrils made from WT  $\alpha$ -synuclein exhibited a banding pattern that was distinct from both the S and NS fibrils (Fig. 6b; Extended Data Fig. 9). Inoculation of TgM83 mice with PMCA fibrils composed of WT  $\alpha$ -synuclein

produced a synucleinopathy that was characterized by neurological symptoms similar to those observed in mice inoculated with either S fibrils or MSA extract, whereas mice injected with monomeric WT  $\alpha$ -synuclein remained asymptomatic (Table 1; Extended Data Fig. 9; Supplementary Videos 9 and 10). After serial passage, the survival curve and incubation periods observed for the PMCA fibril strain were very similar to those observed following passage of the S-fibril-derived strain (Fig. 6c,d). Moreover, the brain regions targeted, the morphology of the cerebral PSyn deposits and the conformational properties of the induced  $\alpha$ -synuclein aggregates in PMCA-fibril-injected TgM83 mice were very similar to those in mice injected with the S-fibril-derived strain (Fig. 6e–g; Extended Data Fig. 9). Thus, not all conformationally distinct recombinant  $\alpha$ -synuclein fibril preparations produce unique disease phenotypes when propagated in TgM83 mice.

**Characterization of  $\alpha$ -synuclein strains from patients with synucleinopathies.** Finally, we looked for strain-specific differences in  $\alpha$ -synuclein aggregates present in brain homogenates from patients with a synucleinopathy. As judged using the CSA, the  $\alpha$ -synuclein aggregates present in patients with MSA were significantly less stable than those present in the brains of patients with DLB or

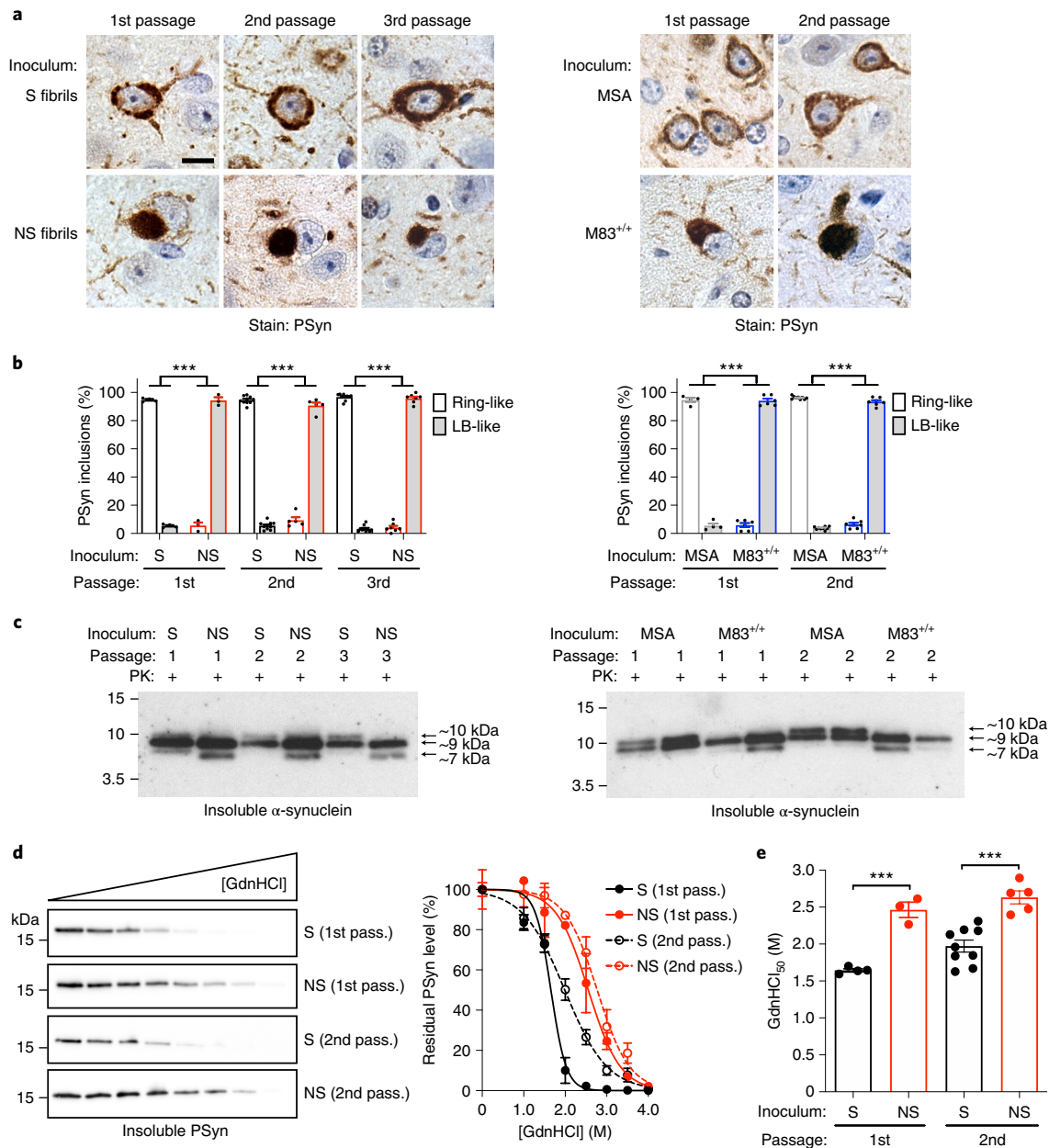


**Fig. 5 | Conformational discrimination of  $\alpha$ -synuclein strains in the brains of inoculated TgM83 mice. a**, Representative immunohistochemistry images of PSyn in the midbrain of clinically ill TgM83 mice inoculated with either the S-fibril-derived or NS-fibril-derived strains (first, second or third passage), or with the MSA-derived or M83<sup>+/+</sup>-derived strains (first or second passage). Neurons in mice inoculated with the S-fibril-derived or MSA-derived strains contain ring-like PSyn deposits, whereas neurons in mice inoculated with the NS-fibril-derived or M83<sup>+/+</sup>-derived strains contain LB-like PSyn deposits. Scale bar, 10  $\mu$ m (applies to all images). **b**, Quantification of ring-like versus LB-like PSyn inclusions in the midbrain of inoculated TgM83 mice. The distribution of PSyn inclusions was significantly different in mice inoculated with the NS-fibril-derived strain compared with mice inoculated with the S-fibril-derived strain ( $***P=5.5 \times 10^{-14}$ ) as well as in mice inoculated with the M83<sup>+/+</sup>-derived strain compared to mice inoculated with the MSA-derived strain ( $***P=2.3 \times 10^{-14}$ ), as determined by one-way ANOVA with Tukey's multiple comparisons test.  $n=5$  (S, first passage), 3 (NS, first passage), 10 (S, second passage), 5 (NS, second passage), 10 (S, third passage), 7 (NS, third passage), 4 (MSA, first passage), 6 (M83<sup>+/+</sup>, first passage), 9 (MSA, second passage) or 7 mice (M83<sup>+/+</sup>, second passage). Data represent the mean  $\pm$  s.e.m. **c**, Immunoblots of detergent-insoluble  $\alpha$ -synuclein species in brain homogenates from inoculated TgM83 mice following treatment with PK. Blots were probed with the Syn-1 antibody. **d**, CSA for PSyn aggregates from TgM83 mice inoculated with either the S-fibril-derived or NS-fibril-derived strains (first or second passage). Representative PSyn immunoblots and the resultant denaturation curves are shown. The curves depict mean residual PSyn values  $\pm$  s.e.m. following treatment with the indicated concentrations of GdnHCl. **e**, The GdnHCl<sub>50</sub> values for PSyn aggregates in mice inoculated with the S-fibril-derived strain are significantly lower than in mice injected with the NS-fibril-derived strain ( $***P=3.3 \times 10^{-4}$  for first passage and  $***P=1.1 \times 10^{-4}$  for second passage, as determined by one-way ANOVA with Tukey's multiple comparisons test). Data represent the mean  $\pm$  s.e.m. For **d** and **e**,  $n=4$  (S, first passage), 3 (NS, first passage), 9 (S, second passage) or 5 mice (NS, second passage).

patients with Alzheimer's disease (AD) with concomitant deposition of  $\alpha$ -synuclein<sup>33</sup> (Fig. 7a,b). As described above and in previous publications<sup>10,11</sup>, brain extracts from patients with MSA transmit

disease to TgM83 mice, with a mean incubation period of ~200 days (Table 1). In contrast, brain extract from a patient with DLB or from a patient with AD, both of which contained thermolysin-resistant

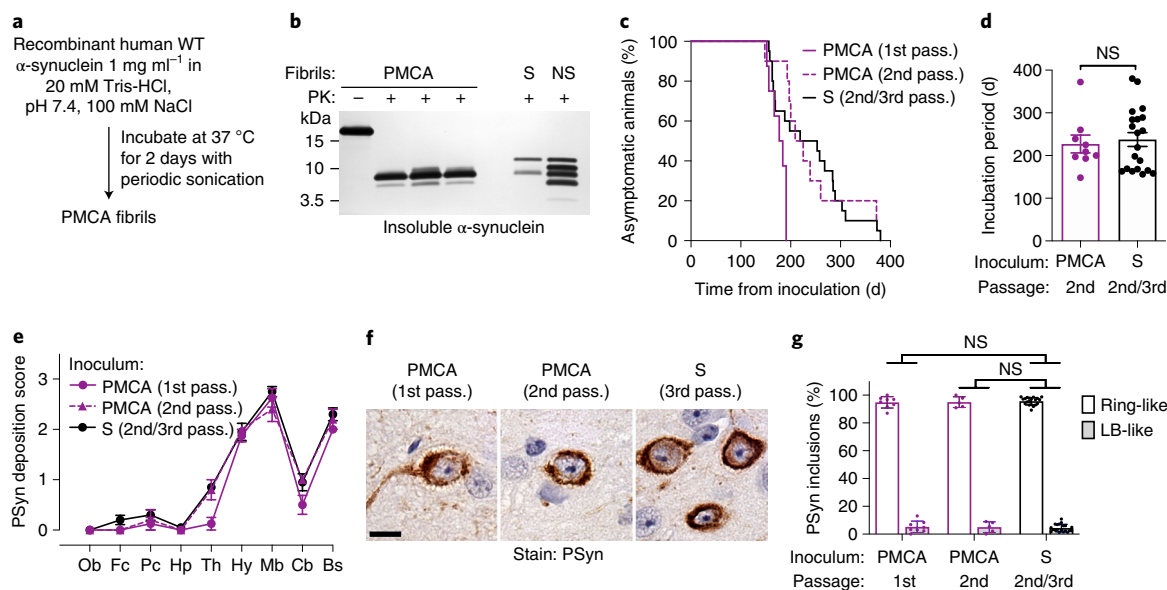


**Fig. 6 | PMCA-generated  $\alpha$ -synuclein fibrils produce a phenotype similar to that induced by S fibrils after propagation in TgM83 mice.** **a**, Schematic of the conditions used for generating PMCA  $\alpha$ -synuclein fibrils. **b**, Following digestion with PK, PMCA fibrils exhibit a different banding pattern of insoluble  $\alpha$ -synuclein species compared to either S or NS fibrils, as assessed by SDS-PAGE followed by silver staining. Results from three independent preparations of PMCA fibrils are shown. **c**, Kaplan-Meier survival curves for TgM83 mice inoculated with the PMCA-fibril-derived strain (first or second passage) or the S-fibril-derived strain (pooled data from second and third passages).  $n = 8$  (PMCA, first passage), 10 (PMCA, second passage) or 20 mice (S, second or third passages). **d**, After the second passage, the incubation periods obtained with the PMCA-derived strain were similar to those for the S-fibril-derived strain (pooled data from second and third passages).  $n = 9$  (PMCA, second passage) or 20 mice (S, second or third passages). Data represent the mean  $\pm$  s.e.m. NS, not significant ( $P = 0.71$  by a two-tailed  $t$ -test). **e**, Semiquantitative PSyn deposition scoring (data represent the mean  $\pm$  s.e.m.) within the indicated brain regions from clinically ill TgM83 mice following inoculation with the PMCA-fibril-derived strain (first or second passage,  $n = 8$  or 5, respectively) or the S-fibril-derived strain (pooled data from second and third passages,  $n = 20$ ). The patterns of PSyn deposition were not significantly different between the three groups ( $P = 0.063$  by two-way ANOVA). **f**, Representative immunohistochemistry images of PSyn in the midbrain of TgM83 mice inoculated with either the PMCA fibril-derived strain (first or second passage) or the S-fibril-derived strain (third passage). The PMCA fibril-derived strain exhibits ring-like PSyn inclusions similar to those present in mice injected with the S-fibril-derived strain. Scale bar, 10  $\mu$ m (applies to all images). **g**, Quantification of ring-like versus LB-like PSyn inclusions in the midbrain of TgM83 mice inoculated with the PMCA-fibril-derived strain ( $n = 8$  for first passage,  $n = 5$  for second passage) compared with mice inoculated with the S-fibril-derived strain (pooled data from second and third passages,  $n = 20$ ). There was no difference in the distribution of ring-like versus LB-like PSyn inclusions between either the first ( $P = 0.80$ ) or second ( $P = 0.91$ ) passages of the PMCA-fibril-derived strain and the S-fibril-derived strain, as determined by one-way ANOVA with Tukey's multiple comparisons test. Data represent the mean  $\pm$  s.e.m.

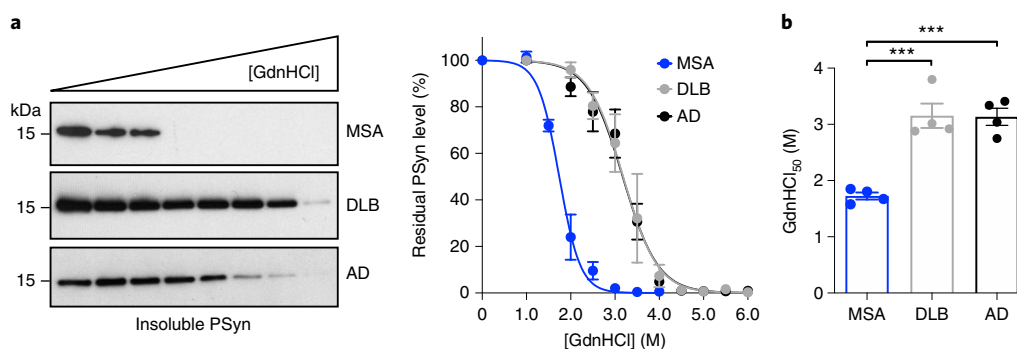


**Fig. 7 | Conformational discrimination of  $\alpha$ -synuclein strains in human synucleinopathies.** **a**, CSA for PSyn aggregates in brain extracts from patients with MSA, DLB or AD with concomitant PSyn deposition. Representative PSyn immunoblots and the resultant denaturation curves are shown. The curves depict mean residual PSyn values  $\pm$  s.e.m. following treatment with the indicated concentrations of GdnHCl. For each disease, samples from four different patients were analyzed. **b**, Significantly higher GdnHCl<sub>50</sub> values were obtained for PSyn aggregates in patients with DLB ( $***P = 3.2 \times 10^{-4}$ ) or AD ( $***P = 3.5 \times 10^{-4}$ ) than for patients with MSA ( $n = 4$  each), as determined by one-way ANOVA with Tukey's multiple comparisons test. Data represent the mean  $\pm$  s.e.m.

$\alpha$ -synuclein (Extended Data Fig. 10), failed to produce neurological illness in TgM83 mice for up to 18 months post-inoculation (Table 1). Moreover, there was no evidence of increased amounts of PSyn deposition in the brains of DLB-inoculated or AD-inoculated

mice compared with mice injected with PBS (Extended Data Fig. 10). Therefore, the investigated DLB and AD brains seem to contain strains of  $\alpha$ -synuclein aggregates that do not propagate efficiently in TgM83 mice.

## Discussion

Here, we showed that  $\alpha$ -synuclein strains, either originating from recombinant fibrils or derived from certain types of synucleinopathy-affected brains, cause distinct synucleinopathies and exhibit the following key features reminiscent of prion strains: (1) variable disease incubation periods after propagation in a mouse model; (2) unique clinical signs of neurological illness; (3) different neuropathological profiles, including variability in regional and cellular vulnerability to protein deposition; (4) distinct conformations of protein aggregates; and (5) the ability to be serially transmitted. Therefore, the existence of  $\alpha$ -synuclein strains provides a plausible explanation for the divergent clinical and pathological disease phenotypes observed among and within the human synucleinopathies. Moreover, these results add to a growing body of literature demonstrating that protein aggregates associated with neurodegenerative diseases, such as those made up of  $\beta$ -amyloid and tau, can exhibit strain-like behavior by specifying distinct phenotypes when propagated in animal models<sup>28,34–38</sup>. The undeniable similarities between  $\alpha$ -synuclein strains and prion strains provide further evidence of the prion-like properties of  $\alpha$ -synuclein aggregates, although it is possible that the specific infectivity of  $\alpha$ -synuclein strains is much lower than that of authentic prion strains.

The different salt concentrations we utilized to generate the S and NS fibril strains are unlikely to explain the genesis of distinct  $\alpha$ -synuclein strains *in vivo*, whereby the cell type in which an aggregate initially forms likely plays a major role in defining its propagation behavior<sup>22</sup>. Nonetheless, the synucleinopathies induced by inoculation of TgM83 mice with S or NS fibrils were markedly different, which indicates that conformational differences within  $\alpha$ -synuclein aggregates underlie the phenotypic heterogeneity. For our *in vivo* propagation studies, we used hemizygous TgM83 mice, which express A53T-mutant  $\alpha$ -synuclein at three to four times the levels found in the brains of non-transgenic mice<sup>26</sup>. We could not detect any mouse  $\alpha$ -synuclein within the induced  $\alpha$ -synuclein aggregates in the inoculated mice, which suggests that high sequence homology between the substrate and the seed is required for efficient  $\alpha$ -synuclein strain propagation. This is in agreement with a study that found that ablation of the mouse  $\alpha$ -synuclein gene in TgM83 mice has no effect on the kinetics of disease following inoculation with MSA<sup>11</sup>. However, others have found that elimination of mouse  $\alpha$ -synuclein promotes the aggregation of human  $\alpha$ -synuclein<sup>39</sup>. While  $\alpha$ -synuclein overexpression in the TgM83 line facilitated our results by allowing observable disease phenotypes (particularly those encoded by the NS fibril and M83<sup>+/+</sup> strains) to occur within the normal lifespan of the mouse, its role, if any, in modulating the strain-like behavior of  $\alpha$ -synuclein aggregates remains to be determined. However, it should be noted that  $\alpha$ -synuclein aggregates can be readily propagated in non-transgenic mice<sup>12</sup>, and  $\alpha$ -synuclein strain-specific effects on tau aggregation can be recapitulated in mice that do not overexpress  $\alpha$ -synuclein<sup>18</sup>.

Different  $\alpha$ -synuclein strains selectively targeted different brain regions and cell types in TgM83 mice, which is reminiscent of the selective targeting observed in the synucleinopathies<sup>15</sup>. There are several potential explanations for this phenomenon. Multiple putative cell surface  $\alpha$ -synuclein receptors have been identified that are capable of facilitating the import of  $\alpha$ -synuclein aggregates into the cell and the initiation of downstream signaling pathways<sup>40–42</sup>. It is conceivable that these receptors could be differentially expressed between cellular populations within the brain and exhibit variable binding affinities for distinct  $\alpha$ -synuclein strains, leading to different rates of aggregate internalization and subsequent propagation. It has also been speculated that cellular differences in  $\alpha$ -synuclein expression level may contribute to selective aggregate vulnerability<sup>43</sup>, and it is possible that different  $\alpha$ -synuclein strains may propagate with differing efficiencies depending on the level of

$\alpha$ -synuclein substrate available. Alternatively, there may be cell-specific and strain-specific differences in rates of  $\alpha$ -synuclein aggregate degradation. Interestingly, we found that inoculation with NS fibrils produced cerebral  $\alpha$ -synuclein deposits in TgM83 mice that were more reminiscent of the LBs found in the brains of patients with PD or DLB than the deposits obtained after inoculation with other types of preformed  $\alpha$ -synuclein fibrils<sup>9</sup>. Moreover, these mice selectively developed  $\alpha$ -synuclein inclusions within the olfactory bulb and cortex, and exhibited  $\alpha$ -synuclein pathology within astrocytes, similar to what occurs in patients with PD or DLB<sup>44,45</sup>. This suggests that TgM83 mice injected with the NS-fibril-derived strain may be a valuable model for investigating PD-related and/or DLB-related disease mechanisms and for assessing candidate therapeutics.

We found that  $\alpha$ -synuclein strains with lower conformational stability, such as those derived from S fibrils or from brain extract from patients with MSA, propagated more rapidly in TgM83 mice than strains with intermediate conformational stability, such as those originating from NS fibrils or M83<sup>+/+</sup> brain extract. Moreover, highly stable  $\alpha$ -synuclein strains, such as those present in the brains of the DLB and AD cases analyzed, failed to cause overt disease when injected into TgM83 mice. This inverse relationship between conformational stability and propagation rate has previously been documented in prion disease<sup>46</sup>. The molecular mechanism underpinning this observation remains to be determined, but could be related to strain-specific differences in rates of aggregate fragmentation and cell-to-cell propagation, as well as susceptibility to cellular degradation. It is easy to conceptualize how smaller, less stable protein aggregates may be able to spread between neighboring cells more efficiently than bulkier, more stable protein aggregates. Indeed, we found that S fibrils were shorter, fragmented at a higher rate and exhibited faster doubling times than NS fibrils. The inability of the S-fibril-derived and MSA-derived strains to sequester  $\alpha$ -synuclein into dense LB-like aggregates may also contribute to their faster propagation rates.

The biochemical and pathological properties of the S-fibril-derived strain (that is, comparatively short disease incubation periods, hindlimb paralysis phenotype, lack of hippocampal PSyn pathology, ring-like PSyn aggregates in neurons and  $\alpha$ -synuclein aggregates with low conformational stability) were similar, if not identical, to those of the MSA strain. Similarly, the properties of the NS-fibril-derived strain (that is, relatively longer disease incubation periods, hindlimb shaking phenotype, abundant hippocampal, cortical and olfactory bulb PSyn pathology, LB-like aggregates in neurons and  $\alpha$ -synuclein aggregates with intermediate conformational stability) were highly reminiscent of the M83<sup>+/+</sup> strain. At the current time, we cannot conclusively determine whether either of these pairs constitutes the same strain as opposed to unique strains with overlapping properties. It is possible that TgM83 mice are only able to replicate a small number of distinct  $\alpha$ -synuclein strains<sup>47</sup>, and that all strains will propagate as either a S-fibril-like or a NS-fibril-like strain depending on their conformational properties. Indeed, PMCA fibrils, which possess biochemical characteristics that are distinct from both S and NS fibrils, produced a disease phenotype indistinguishable from that of S fibrils following propagation in TgM83 mice. Hence,  $\alpha$ -synuclein strains may be composed of an ensemble or 'cloud' of distinct conformational states, similar to what has been proposed for prion strains<sup>48</sup>. Propagation of recombinant  $\alpha$ -synuclein strains in TgM83 mice may lead to the selection of a minor component of the ensemble that is more compatible with the new host. This could also explain why  $\alpha$ -synuclein aggregates in patients with MSA are predominantly found within oligodendrocytes, whereas MSA-inoculated TgM83 mice exhibit only neuronal  $\alpha$ -synuclein pathology<sup>10,11</sup>.

Two potential hypotheses have been put forward to explain the apparent spreading of  $\alpha$ -synuclein aggregates within the brains of patients with PD<sup>49,50</sup>. The first, the selective neuronal vulnerability hypothesis, contends that  $\alpha$ -synuclein aggregates appear first in

cells that are most vulnerable to disease-associated toxicity and then appear later in less vulnerable cells once the disease has advanced. The second mechanism, the prion-like propagation theory, argues that  $\alpha$ -synuclein aggregates directly transfer between neurons, acting as seeds for the generation of new aggregates in recipient cells. That the conformational and pathological properties of  $\alpha$ -synuclein strains were faithfully maintained following serial propagation argues that prion-like conformational templating, which requires physical contact between the seed and the substrate, occurred. However, the differential cellular tropism of  $\alpha$ -synuclein strains argues that not all cells are equally susceptible to developing specific types of  $\alpha$ -synuclein pathology. Thus, our results suggest that both prion-like spreading and selective vulnerability contribute to the temporal and spatial evolution of  $\alpha$ -synuclein pathology within the brain.

### Online content

Any methods, additional references, Nature Research reporting summaries, source data, extended data, supplementary information, acknowledgements, peer review information; details of author contributions and competing interests; and statements of data and code availability are available at <https://doi.org/10.1038/s41593-019-0541-x>.

Received: 13 July 2018; Accepted: 18 October 2019;

Published online: 2 December 2019

### References

- Spillantini, M. G. & Goedert, M. The  $\alpha$ -synucleinopathies: Parkinson's disease, dementia with Lewy bodies, and multiple system atrophy. *Ann. NY Acad. Sci.* **920**, 16–27 (2000).
- Burre, J. et al.  $\alpha$ -Synuclein promotes SNARE-complex assembly in vivo and in vitro. *Science* **329**, 1663–1667 (2010).
- Fujiwara, H. et al.  $\alpha$ -Synuclein is phosphorylated in synucleinopathy lesions. *Nat. Cell Biol.* **4**, 160–164 (2002).
- Lashuel, H. A., Overk, C. R., Oueslati, A. & Masliah, E. The many faces of  $\alpha$ -synuclein: from structure and toxicity to therapeutic target. *Nat. Rev. Neurosci.* **14**, 38–48 (2013).
- Polymeropoulos, M. H. et al. Mutation in the  $\alpha$ -synuclein gene identified in families with Parkinson's disease. *Science* **276**, 2045–2047 (1997).
- Jucker, M. & Walker, L. C. Propagation and spread of pathogenic protein assemblies in neurodegenerative diseases. *Nat. Neurosci.* **21**, 1341–1349 (2018).
- Schechel, C. & Aguzzi, A. Prions, prionoids and protein misfolding disorders. *Nat. Rev. Genet.* **19**, 405–418 (2018).
- Mougenot, A. L. et al. Prion-like acceleration of a synucleinopathy in a transgenic mouse model. *Neurobiol. Aging* **33**, 2225–2228 (2012).
- Luk, K. C. et al. Intracerebral inoculation of pathological  $\alpha$ -synuclein initiates a rapidly progressive neurodegenerative  $\alpha$ -synucleinopathy in mice. *J. Exp. Med.* **209**, 975–986 (2012).
- Watts, J. C. et al. Transmission of multiple system atrophy prions to transgenic mice. *Proc. Natl Acad. Sci. USA* **110**, 19555–19560 (2013).
- Prusiner, S. B. et al. Evidence for  $\alpha$ -synuclein prions causing multiple system atrophy in humans with parkinsonism. *Proc. Natl Acad. Sci. USA* **112**, E5308–E5317 (2015).
- Luk, K. C. et al. Pathological  $\alpha$ -synuclein transmission initiates Parkinson-like neurodegeneration in nontransgenic mice. *Science* **338**, 949–953 (2012).
- Masuda-Suzukake, M. et al. Prion-like spreading of pathological  $\alpha$ -synuclein in brain. *Brain* **136**, 1128–1138 (2013).
- Peng, C., Gathagan, R. J. & Lee, V. M. Distinct  $\alpha$ -synuclein strains and implications for heterogeneity among  $\alpha$ -synucleinopathies. *Neurobiol. Dis.* **109**, 209–218 (2018).
- Alegre-Abarrategui, J. et al. Selective vulnerability in  $\alpha$ -synucleinopathies. *Acta Neuropathol.* **38**, 681–704 (2019).
- Morales, R., Abid, K. & Soto, C. The prion strain phenomenon: molecular basis and unprecedented features. *Biochim. Biophys. Acta* **1772**, 681–691 (2007).
- Telling, G. C. et al. Evidence for the conformation of the pathologic isoform of the prion protein enciphering and propagating prion diversity. *Science* **274**, 2079–2082 (1996).
- Guo, J. L. et al. Distinct  $\alpha$ -synuclein strains differentially promote tau inclusions in neurons. *Cell* **154**, 103–117 (2013).
- Bousset, L. et al. Structural and functional characterization of two  $\alpha$ -synuclein strains. *Nat. Commun.* **4**, 2575 (2013).
- Peelaerts, W. et al.  $\alpha$ -Synuclein strains cause distinct synucleinopathies after local and systemic administration. *Nature* **522**, 340–344 (2015).
- Woerman, A. L. et al. Propagation of prions causing synucleinopathies in cultured cells. *Proc. Natl Acad. Sci. USA* **112**, E4949–E4958 (2015).
- Peng, C. et al. Cellular milieu imparts distinct pathological  $\alpha$ -synuclein strains in  $\alpha$ -synucleinopathies. *Nature* **557**, 558–563 (2018).
- Yamasaki, T. R. et al. Parkinson's disease and multiple system atrophy have distinct  $\alpha$ -synuclein seed characteristics. *J. Biol. Chem.* **294**, 1045–1058 (2019).
- Candelise, N. et al. Seeding variability of different alpha synuclein strains in synucleinopathies. *Ann. Neurol.* **85**, 691–703 (2019).
- Woerman, A. L. et al. Multiple system atrophy prions retain strain specificity after serial propagation in two different Tg(SNCA\* A53T) mouse lines. *Acta Neuropathol.* **137**, 437–454 (2019).
- Giasson, B. I. et al. Neuronal  $\alpha$ -synucleinopathy with severe movement disorder in mice expressing A53T human  $\alpha$ -synuclein. *Neuron* **34**, 521–533 (2002).
- Froula, J. M. et al. Defining  $\alpha$ -synuclein species responsible for Parkinson's disease phenotypes in mice. *J. Biol. Chem.* **294**, 10392–10406 (2019).
- Condello, C. et al. Structural heterogeneity and intersubject variability of A $\beta$  in familial and sporadic Alzheimer's disease. *Proc. Natl Acad. Sci. USA* **115**, E782–E791 (2018).
- Holmes, B. B. et al. Proteopathic tau seeding predicts tauopathy in vivo. *Proc. Natl Acad. Sci. USA* **111**, E4376–E4385 (2014).
- Sang, J. C. et al. Direct observation of murine prion protein replication in vitro. *J. Am. Chem. Soc.* **140**, 14789–14798 (2018).
- Aoki, N. et al. Atypical multiple system atrophy is a new subtype of frontotemporal lobar degeneration: frontotemporal lobar degeneration associated with  $\alpha$ -synuclein. *Acta Neuropathol.* **130**, 93–105 (2015).
- Herva, M. E. et al. Anti-amyloid compounds inhibit  $\alpha$ -synuclein aggregation induced by protein misfolding cyclic amplification (PMCA). *J. Biol. Chem.* **289**, 11897–11905 (2014).
- Hamilton, R. L. Lewy bodies in Alzheimer's disease: a neuropathological review of 145 cases using  $\alpha$ -synuclein immunohistochemistry. *Brain Pathol.* **10**, 378–384 (2000).
- Heilbronner, G. et al. Seeded strain-like transmission of  $\beta$ -amyloid morphotypes in APP transgenic mice. *EMBO Rep.* **14**, 1017–1022 (2013).
- Watts, J. C. et al. Serial propagation of distinct strains of A $\beta$  prions from Alzheimer's disease patients. *Proc. Natl Acad. Sci. USA* **111**, 10323–10328 (2014).
- Rasmussen, J. et al. Amyloid polymorphisms constitute distinct clouds of conformational variants in different etiological subtypes of Alzheimer's disease. *Proc. Natl Acad. Sci. USA* **114**, 13018–13023 (2017).
- Sanders, D. W. et al. Distinct tau prion strains propagate in cells and mice and define different tauopathies. *Neuron* **82**, 1271–1288 (2014).
- Clavaguera, F. et al. Brain homogenates from human tauopathies induce tau inclusions in mouse brain. *Proc. Natl Acad. Sci. USA* **110**, 9535–9540 (2013).
- Fares, M. B. et al. Induction of de novo  $\alpha$ -synuclein fibrillization in a neuronal model for Parkinson's disease. *Proc. Natl Acad. Sci. USA* **113**, E912–E921 (2016).
- Holmes, B. B. et al. Heparan sulfate proteoglycans mediate internalization and propagation of specific proteopathic seeds. *Proc. Natl Acad. Sci. USA* **110**, E3138–E3147 (2013).
- Mao, X. et al. Pathological  $\alpha$ -synuclein transmission initiated by binding lymphocyte-activation gene 3. *Science* **353**, aah3374 (2016).
- Ferreira, D. G. et al.  $\alpha$ -Synuclein interacts with PrP<sup>C</sup> to induce cognitive impairment through mGluR5 and NMDAR2B. *Nat. Neurosci.* **20**, 1569–1579 (2017).
- Luna, E. et al. Differential  $\alpha$ -synuclein expression contributes to selective vulnerability of hippocampal neuron subpopulations to fibril-induced toxicity. *Acta Neuropathol.* **135**, 855–875 (2018).
- Sorrentino, Z. A., Giasson, B. I. & Chakrabarty, P.  $\alpha$ -Synuclein and astrocytes: tracing the pathways from homeostasis to neurodegeneration in Lewy body disease. *Acta Neuropathol.* **138**, 1–21 (2019).
- Beach, T. G. et al. Olfactory bulb  $\alpha$ -synucleinopathy has high specificity and sensitivity for Lewy body disorders. *Acta Neuropathol.* **117**, 169–174 (2009).
- Legname, G. et al. Continuum of prion protein structures enciphers a multitude of prion isolate-specified phenotypes. *Proc. Natl Acad. Sci. USA* **103**, 19105–19110 (2006).
- Dhillon, J. S. et al. Comparative analyses of the in vivo induction and transmission of  $\alpha$ -synuclein pathology in transgenic mice by MSA brain lysate and recombinant  $\alpha$ -synuclein fibrils. *Acta Neuropathol. Commun.* **7**, 80 (2019).
- Collinge, J. & Clarke, A. R. A general model of prion strains and their pathogenicity. *Science* **318**, 930–936 (2007).
- Walsh, D. M. & Selkoe, D. J. A critical appraisal of the pathogenic protein spread hypothesis of neurodegeneration. *Nat. Rev. Neurosci.* **17**, 251–260 (2016).
- Surmeier, D. J., Obeso, J. A. & Halliday, G. M. Selective neuronal vulnerability in Parkinson disease. *Nat. Rev. Neurosci.* **18**, 101–113 (2017).

**Publisher's note** Springer Nature remains neutral with regard to jurisdictional claims in published maps and institutional affiliations.

© The Author(s), under exclusive licence to Springer Nature America, Inc. 2019

## Methods

**Expression and purification of recombinant  $\alpha$ -synuclein.** Untagged full-length human  $\alpha$ -synuclein (residues 1–140), either WT or containing the A53T mutation, was inserted into the pET-28a vector (EMD Millipore) and then expressed and purified from *Escherichia coli* strain BL21(DE3) using an established protocol<sup>51</sup>. Briefly,  $\alpha$ -synuclein expression was induced for 2.5 h using isopropyl  $\beta$ -D-1-thiogalactopyranoside (IPTG) and then cell pellets were collected by centrifugation at 5,000  $\times$ g. Pellets were washed in PBS and then spun down again at the same speed. Next, pellets were resuspended in PBS containing 1 mM phenylmethylsulfonyl fluoride (PMSF), lysed using a tip sonicator (18% amplitude, 6 pulses of 25 s with 2 min of rest on ice in between), and then boiled for 15 min. Debris was pelleted by centrifugation at 10,000 g for 10 min, and then the supernatant was clarified by ultracentrifugation (150,000 g for 30 min) followed by dialysis against 50 mM Tris-HCl, pH 8.3.  $\alpha$ -Synuclein was then purified by fast protein liquid chromatography using a Mono Q anion exchange column (GE Healthcare) and eluted using a linear gradient of 0 to 500 mM NaCl in 50 mM Tris-HCl, pH 8.3. The purity of eluted fractions was analyzed by SDS-PAGE and Coomassie blue staining, and then fractions of sufficient purity were pooled and dialyzed against 20 mM Tris-HCl, pH 7.4. The concentration of purified  $\alpha$ -synuclein was determined by measuring the absorbance at 280 nm using a NanoDrop spectrophotometer (extinction coefficient of 5,960 M<sup>-1</sup> cm<sup>-1</sup>), and then the purified protein was aliquoted, flash frozen and stored at  $-80^{\circ}$ C.

**Generation of  $\alpha$ -synuclein fibrils.** Our goal was to produce different preparations of recombinant  $\alpha$ -synuclein fibrils that exhibited divergent conformational properties. To this end, we screened several different buffers and found that polymerization in the presence or absence of sodium chloride produced conformationally unique fibrils. S and NS fibrils were generated by incubating recombinant  $\alpha$ -synuclein at a concentration of 1 mg ml<sup>-1</sup> (69  $\mu$ M) at 37  $^{\circ}$ C with continuous shaking (600 r.p.m. using an Eppendorf Thermomixer F1.5) for 7 days. S fibrils were prepared in a buffer containing 20 mM Tris-HCl, pH 7.4 and 100 mM NaCl whereas NS fibrils were prepared in a buffer containing 20 mM Tris-HCl, pH 7.4. Fibril formation was confirmed using a ThT fluorescence assay. Briefly, fibrils were diluted in a buffer containing 10  $\mu$ M ThT (Sigma-Aldrich, T3516) and then fluorescence was measured using excitation and emission wavelengths of 444 nm and 485 nm, respectively. To analyze the kinetics of fibril formation for S and NS fibrils, recombinant  $\alpha$ -synuclein (1 mg ml<sup>-1</sup>) was prepared in 20 mM Tris-HCl, pH 7.4 and 10  $\mu$ M ThT with or without the addition of 100 mM NaCl. Protein was placed into the wells of a black 96-well clear-bottom microplate and then the plate was inserted into a BMG CLARIOstar microplate reader. Samples were incubated at 37  $^{\circ}$ C with continuous shaking (600 r.p.m., double orbital) for 12 days and ThT fluorescence (excitation of 444  $\pm$  5 nm, emission of 485  $\pm$  5 nm) was measured every 5 min. A gain setting of 1,500 was used. Nonlinear regression was used to fit the kinetic curves to a sigmoidal dose-response (variable slope) equation in GraphPad Prism, and then lag phases were calculated using the following equation:  $T_{50} = [1/(2 \times k)]$ , where  $T_{50}$  is the time at which fluorescence is halfway between the baseline and plateau values, and  $k$  is the Hill slope. Lag phases were compared using a two-tailed, unpaired  $t$ -test. ThT fluorescence values at different timepoints were compared by two-way analysis of variance (ANOVA) with Sidak's multiple comparisons test.

PMCA fibrils were generated by preparing recombinant  $\alpha$ -synuclein at a concentration of 1 mg ml<sup>-1</sup> in a buffer containing 20 mM Tris-HCl, pH 7.4 and 100 mM NaCl. Samples were placed in thin-walled PCR microtubes and then positioned in a microtube holder (QSonica, 444) suspended over a microplate horn sonicator (QSonica, 431MPX). The bottoms of the tubes were submerged in water that was kept at 37  $^{\circ}$ C and was continually circulated for the duration of the experiment using a recirculating chiller (QSonica, 4900–110). Samples were subjected to repeating cycles of 29 min 40 s of incubation and 20 s of sonication (70% amplitude using a QSonica Q700 sonicator) over a period of 2 days.

**Electron microscopy.** Negative-stain electron microscopy was used to examine the ultrastructural characteristics of S, NS and PMCA fibrils. Aliquots (5  $\mu$ l of 69  $\mu$ M  $\alpha$ -synuclein fibril preparations) containing recombinant  $\alpha$ -synuclein fibrils were loaded onto freshly glow-discharged 400 mesh carbon-coated copper grids (Electron Microscopy Sciences) and adsorbed for 1 min. Grids were then washed with 50  $\mu$ l each of 0.1 M and 0.01 M ammonium acetate and stained with 2  $\times$  50  $\mu$ l of freshly filtered 2% uranyl acetate. Once dry, grids were visualized using a Technai G20 transmission electron microscope (Thermo Fisher FEI) using an acceleration voltage of 200 kV. Electron micrographs were recorded using an Eagle 4kx4k CCD camera (Thermo Fisher FEI). Fibril lengths were measured from a total of 62 S fibrils and 47 NS fibrils stemming from 3 independent fibril preparations. No overlapping or otherwise obscured fibrils were included in the length measurements. Measurements were determined in Adobe Photoshop software using the Ruler tool, which allows single pixel accuracy in the measurements with  $\sim$ 0.5 nm per pixel at the image magnification that was used. Mean fibril lengths from three independent preparations were compared using a two-tailed, unpaired  $t$ -test.

**PK digestion of fibrils.** Fibrils were diluted into 1  $\times$  detergent buffer (0.5% (v/v) Nonidet P-40, 0.5% (w/v) sodium deoxycholate in PBS) containing PK (Thermo

Scientific, EO0491) at a concentration of 50  $\mu$ g ml<sup>-1</sup> (PK/protein ratio of 1:1) and then incubated at 37  $^{\circ}$ C for 1 h with continuous shaking. Digestions were halted by adding PMSF to a final concentration of 4 mM and then samples were ultracentrifuged at 100,000 g for 1 h at 4  $^{\circ}$ C. The supernatant was discarded, and the pellets were resuspended by boiling in 1  $\times$  Bolt lithium dodecyl sulfate sample buffer (Thermo Scientific) containing 2.5% (v/v)  $\beta$ -mercaptoethanol (loading buffer). Samples were then analyzed by SDS-PAGE followed by silver staining.

**SDS-PAGE and immunoblotting.** Samples were prepared in loading buffer, boiled and then run on 4–12%, 10% or 12% Bolt Bis-Tris Plus gels (Thermo Scientific) at 165 V for 35 min. A Thermo Scientific Pierce Silver Stain kit and Bio-Safe Coomassie stain (Bio-Rad) were used for silver staining and Coomassie blue staining, respectively. For immunoblotting, proteins were transferred to 0.45  $\mu$ m-pore polyvinylidene fluoride membranes in transfer buffer (25 mM Tris buffer, pH 8.3, 0.192 M glycine, 20% (v/v) methanol) at 35 V for 1 h. The membranes were then incubated in 0.4% (v/v) paraformaldehyde in PBS for 30 min at room temperature to crosslink proteins to the membrane<sup>52</sup>. Membranes were blocked with blocking buffer (5% (w/v) skim milk in 1  $\times$  TBS containing 0.05% (v/v) Tween-20 (TBST)) for 1 h at room temperature and then incubated overnight at 4  $^{\circ}$ C with primary antibody diluted in blocking buffer. The following primary antibodies were used: anti-Ser129-Psyn EP1536Y (Abcam, ab51253; 1:4,000 dilution); anti- $\alpha$ -synuclein Syn-1 (BD Biosciences, 610786; 1:10,000 dilution); anti-human  $\alpha$ -synuclein MJFR1 (Abcam, ab138501; 1:10,000 dilution); or anti-murine  $\alpha$ -synuclein D37A6 (Cell Signaling Technology, 4179; 1:10,000 dilution). Following three washes with TBST, the membranes were incubated with horseradish-peroxidase-conjugated secondary antibodies (Bio-Rad, 172–1019 or 172–1011) diluted 1:10,000 in blocking buffer for 1 h at room temperature. Following three washes with TBST, blots were developed using Western Lightning enhanced chemiluminescence (ECL) Pro (PerkinElmer) and either exposed to X-ray film or imaged using a LiCor Odyssey Fc system.

**Curcumin-dye-binding assay.** Based on the recent demonstration that curcumin can be used as a conformation-sensitive probe for discriminating different types of amyloid- $\beta$  fibrils<sup>28</sup>, we developed a fluorescence spectral assay for  $\alpha$ -synuclein fibrils using this dye. Reactions were prepared using 10  $\mu$ M  $\alpha$ -synuclein (S fibrils, NS fibrils or nonpolymerized  $\alpha$ -synuclein prepared in matching buffer) and curcumin (Sigma-Aldrich, C1386) at a final concentration of 5  $\mu$ M in a total volume of 100  $\mu$ l. Samples were then incubated at room temperature with shaking (850 r.p.m.) for 15 min. Unbound dye was removed by dialyzing against dH<sub>2</sub>O for  $\sim$ 50 min using Slide-A-Lyzer Mini dialysis tubes with a 10-kDa molecular weight cut-off (Thermo Scientific, 69570). Samples were then placed into black 96-well clear-bottom half-area plates (Greiner), and fluorescence emission spectra (460  $\pm$  5 nm to 625  $\pm$  5 nm) following excitation at 432  $\pm$  7.5 nm were recorded using a BMG CLARIOstar microplate reader, with the gain set at 2,000. Background fluorescence was subtracted using samples containing only curcumin that had been identically processed. For comparison of spectra, fluorescence values were normalized to the highest signal obtained within the spectrum (which was set at 1.0).

**Cultured cell  $\alpha$ -synuclein aggregation assay.** A polyclonal HEK293 cell line stably expressing A53T-mutant human  $\alpha$ -synuclein tagged at its C terminus with YFP<sup>29</sup> was provided by M. Diamond (UT Southwestern). These cells were cultured in growth medium (DMEM containing 10% (v/v) fetal bovine serum, 1  $\times$  GlutaMAX and 0.2  $\times$  penicillin-streptomycin) and maintained in a humidified 37  $^{\circ}$ C/5% CO<sub>2</sub> environment. For fibril transductions, equal volumes of Lipofectamine-2000 (Thermo Scientific) and  $\alpha$ -synuclein fibril solutions, both diluted in Opti-MEM medium, were combined to give final concentrations of 2.8% (v/v) Lipofectamine-2000 and 1  $\mu$ M total  $\alpha$ -synuclein, and then incubated for 20 min to allow liposome formation. During this incubation, cells were trypsinized and then plated at a density of 20,000 cells per well in 24-well plates containing coverslips coated with poly-D-lysine. Transduction mixture (200  $\mu$ l per well) was added and then the cells were incubated for 4 h. The transduction medium was then removed and, without additional washes, replaced with growth medium and returned to the incubator for an additional 20 h. Cells were fixed with methanol at  $-30^{\circ}$ C for 15 min, washed 3 times with PBS, and the coverslips were mounted on glass slides with ProLong Diamond Antifade Mountant containing 4',6'-diamidino-2-phenylindole (DAPI; Thermo Scientific). Slides were allowed to dry overnight and then imaged using a Leica TCS SP8 confocal microscope. Images were processed using ImageJ and Adobe Photoshop.

For quantification of aggregate morphology, fibril-transduced cells were prepared as above with the exception that cells were fixed with 4% (w/v) paraformaldehyde for 15 min. Slides were viewed using a  $\times$ 40 objective on a Leica DM6000B microscope. For each replicate, four random fields were chosen and the number of aggregates exhibiting the 'globular' or 'thread-like' morphology were counted. These values were summed and converted to percentage of total aggregates. For both S-fibril-treated and NS-fibril-treated cells, four independent replicates were analyzed. Aggregate morphologies were compared using a two-tailed  $t$ -test.

**Fibril CSA.** Twenty microliters of 2  $\times$  GdnHCl stocks were added to an equal volume of recombinant  $\alpha$ -synuclein fibrils (5  $\mu$ l of 1 mg ml<sup>-1</sup> fibrils plus 15  $\mu$ l

of detergent buffer) to generate final GdnHCl concentrations of 1, 1.5, 2, 2.5, 3, 3.5 and 4 M. To generate the 0 M GdnHCl sample, 20  $\mu$ l of dH<sub>2</sub>O was added. Samples were then incubated at room temperature for 2 h with continuous shaking (800 r.p.m.). GdnHCl concentrations were then normalized to 0.4 M and the samples were ultracentrifuged at 100,000 g for 1 h at 4 °C using a TLA-55 rotor (Beckman). Supernatants were discarded and the pellets resuspended by boiling in loading buffer. Levels of residual  $\alpha$ -synuclein were determined by SDS-PAGE followed by either immunoblotting or Coomassie blue staining. Densitometry was performed using ImageJ, and values were normalized to the sample with the highest intensity, which was set at 100%. GdnHCl<sub>50</sub> values, the concentration of GdnHCl at which 50% of the aggregates are solubilized, were determined by nonlinear regression using the sigmoidal dose-response (variable slope) equation in GraphPad Prism, with the top and bottom values fixed at 100 and 0, respectively. GdnHCl<sub>50</sub> values were compared using a two-tailed, unpaired *t*-test. To generate denaturation curves, values for independent replicates were averaged and then normalized to the 0 M GdnHCl value, which was set at 100%.

**Single-molecule measurement of  $\alpha$ -synuclein fibril doubling time.** Fibril seeds were sonicated for 1 min at 60 W power and then added at a concentration of 0.35% (w/v) to a 300  $\mu$ l solution of monomeric recombinant A53T-mutant  $\alpha$ -synuclein (70  $\mu$ M) prepared in PBS containing 0.01% (v/v) sodium azide. Seeding reactions were carried out at 37 °C with continuous shaking (200 r.p.m.), and aliquots were withdrawn at defined timepoints for analysis by TIRF microscopy. Protein aliquots were diluted to a final concentration of 100 nM in PBS containing 25  $\mu$ M ThT and then loaded onto a slide. Borosilicate glass coverslips were cleaned by argon plasma for 1 h and then attached to Frame-Seal slide chambers (9  $\times$  9 mm), with the surface coated with poly-L-lysine (molecular weight of 150,000–300,000, 0.01% (v/v)). Imaging was performed using a custom-built TIRF microscopy setup. A 35-mW diode laser with a wavelength of 405 nm was passed through a single-band bandpass filter then directed into a  $\times$ 60 magnification oil-immersion TIRF objective (numerical aperture of 1.49) mounted on an inverted microscope. The TIRF mode was achieved by adjusting the position of the aligned laser beam before it entered the objective, illuminating samples mixed with ThT molecules. The emitted fluorescence was collected by the same objective, separated by a dichroic mirror from the returning TIR beam and then passed through an emission filter. The fluorescence signal was recorded using an EMCCD camera. Each recorded area contained a 3  $\times$  3 grid (that is, 9 images were recorded sequentially at adjacent positions), in which the dimensions of a single image were 512  $\times$  512 pixels (that is, 110  $\times$  110  $\mu$ m<sup>2</sup>), with a gap distance of 150  $\mu$ m. For each timepoint in the kinetic measurements, three random areas (that is, 27 images) were recorded. Each image sequence was acquired as a 100-frame stack at 30 frames s<sup>-1</sup>. Individual image data were averaged over all the frames using ImageJ (<http://imagej.nih.gov/ij/>), and the images were then analyzed using a custom-written Matlab script, which has been uploaded to Github (<https://github.com/jason82133/Particle-measurement.git>). For particle identification, background was removed by applying two-dimensional Gaussian blur and bandpass filters. Boundaries for individual particles were identified by applying a black/white filter (that is, an intensity threshold), while their positions were located by calculating centroid positions. Particle length was measured using built-in algorithms by thinning individual boundaries of particles and then calculated with the image pixel size of 235 nm.

To extract multiplication rates from the in vitro data of average length as a function of time, the system was modeled using the differential equations describing linear polymerization with monomer concentration-independent multiplication<sup>53</sup> as follows:

$$\frac{dM}{dt} = 2(k_e m(t) - k_{off})P(t)$$

$$\frac{dP}{dt} = k_f M(t)$$

where  $M(t)$  is the mass concentration of aggregates and  $P(t)$  is the number concentration of aggregates. Thus, the average number of monomers per aggregate is given by  $M(t)/P(t)$ .  $k_e$ ,  $k_{off}$  and  $k_f$  are the rate constants of elongation, depolymerization and fragmentation respectively. From these constants, the doubling time ( $t_2$ ), that is, the time taken to double the number of aggregates at a given monomer concentration  $m$ , is given by

$$t_2 = \frac{\ln(2)}{\sqrt{2k_e m k_f}}$$

To convert the measured length (in nm) to the number of monomers per aggregate, an additional parameter, the number of monomers per unit length of fibril, was needed (relative differences between the multiplication rate are insensitive to the precise value of this parameter as long as it is the same for the systems being compared). The data were fit by numerical integration of the above differential equations, with three free-fitting parameters ( $k_e$ ,  $k_f$  and the number of monomers per unit length of the fibril). The depolymerization rate was expressed in terms of the monomer concentration at equilibrium, and the elongation rate  $k_{off} = m_{equ} \times k_e$ , thus reducing the number of fitting parameters to three overall. The initial concentration of fibrils,  $M(t=0)$ , was 0.245  $\mu$ M and the initial fibril length was determined from the average length at time 0.

**Mice.** Homozygous M83 transgenic mice (M83<sup>+/+</sup>), which express A53T-mutant human  $\alpha$ -synuclein under the control of the mouse prion protein promoter<sup>66</sup> on a mixed C57BL/6/C3H background, and B6C3F1 non-transgenic mice were purchased from The Jackson Laboratories (stock numbers 004479 and 100010, respectively). These two lines were intercrossed to generate hemizygous TgM83 mice, which were housed at four to five animals per cage. Mice were maintained on a 12 h light–12 h dark cycle and were given unlimited access to food and water. All mouse experiments were performed in accordance with guidelines set by the Canadian Council on Animal Care under a protocol (AUP number 4263.6) approved by the University Health Network Animal Care Committee.

**Tissue samples.** Human synucleinopathy samples were provided by the Massachusetts Alzheimer's Disease Research Center, and AD samples were obtained from the Canadian Brain Tissue Bank. Informed consent was obtained at the point of tissue collection. A list of the brain tissues used is given in Supplementary Table 2. The use of human tissue was in accordance with guidelines provided by the University of Toronto, and all relevant ethical regulations were followed. Spontaneously ill M83<sup>+/+</sup> mice were killed once prominent hindlimb paralysis and bradykinesia and concomitant weight loss were observed. Mice were perfused with saline, and then the brain was removed and bisected parasagittally. The right half of the brain was fixed in 10% neutral buffered formalin and the left half was frozen and stored at –80 °C. The M83<sup>+/+</sup> sample used for inoculation studies was from a male mouse that was killed at 371 days of age. Brain homogenates from frozen MSA, DLB, AD or M83<sup>+/+</sup> tissue (10% (w/v) prepared in calcium-free and magnesium-free PBS) were generated using a Minilys homogenizer and CK14 soft tissue homogenizing tubes (Bertin). Homogenates were aliquoted and then stored at –80 °C.

**Intracerebral inoculations.** Inoculations were performed as follows: ~5-week-old hemizygous M83 mice were anesthetized and then inoculated non-sterilely using a tuberculin syringe with an attached 27 gauge, 0.5-inch needle (BD Biosciences, 305945) with 30  $\mu$ l of sample at a depth of ~3 mm into the right cerebral hemisphere of the brain. This region corresponds to the hippocampus or thalamus. For inoculations with recombinant  $\alpha$ -synuclein preparations (S fibrils, NS fibrils or monomeric  $\alpha$ -synuclein), each mouse received 1  $\mu$ g of total  $\alpha$ -synuclein diluted in inoculum diluent buffer (5% (w/v) BSA prepared in sterile PBS). For PBS inoculations, sterile PBS was diluted 1:10 in inoculum diluent buffer before inoculation. For inoculations with brain-derived samples, homogenates were diluted to 1% (w/v) in inoculum diluent buffer before injection. For serial passaging experiments, brain homogenates from previously inoculated hemizygous TgM83 mice were used. We estimated that for the serial transmission experiments, mice received approximately tenfold less  $\alpha$ -synuclein aggregates than for the original fibril inoculations. Both male and female mice were used for inoculation studies. The sex distribution for individual experiments is shown in Supplementary Table 3. Mice were randomly assigned to the experimental groups. No statistical methods were used to predetermine mouse numbers for inoculation experiments, but our sample sizes were similar to those reported in previous publications<sup>10,11</sup>. Inoculated mice were monitored daily for routine health and assessed two to three times per week for signs of neurological illness. Mice were killed after progressing to end-stage disease, which was defined as either prominent hindlimb paralysis with reduced ambulation or hindlimb shaking accompanied by obvious weight loss and kyphosis. Disease incubation periods were compared by one-way ANOVA with Tukey's multiple comparisons test. Following transcardiac perfusion with saline solution, brains were divided parasagittally. The left half of the brain was frozen and stored at –80 °C for biochemical experiments, and the right half was fixed in 10% neutral buffered formalin for neuropathology. Some inoculated mice were found dead in the absence of neurological signs or were killed due to intercurrent illness (Supplementary Table 4). These mice were omitted from the study.

**Protease digestion assays.** Brain homogenates (10% (w/v)) were prepared in PBS using a Minilys homogenizer and CK14 homogenizing tubes. Nine volumes of brain homogenate were then mixed with one volume of 10 $\times$  detergent buffer (5% (v/v) Nonidet P-40, 5% (w/v) sodium deoxycholate in PBS) containing Pierce Universal Nuclease (ThermoFisher, 88701) and Halt Phosphatase Inhibitor (ThermoFisher, 78420) and then incubated on ice for 20 min. Samples were clarified by centrifugation at 1,000 g for 5 min at 4 °C to generate detergent-extracted brain homogenate. For thermolysin (Sigma-Aldrich, T7902) digestions, extracts were treated with 50  $\mu$ g ml<sup>-1</sup> protease (thermolysin/protein ratio of 1:100) at 37 °C for 1 h with constant agitation (600 r.p.m.). Digestions were terminated by the addition of EDTA to a final concentration of 5 mM. For PK digestions, detergent-extracted brain homogenates were treated with 100  $\mu$ g ml<sup>-1</sup> PK (PK/protein ratio of 1:50) at 37 °C for 1 h with constant agitation (600 r.p.m.). Digestions were terminated by the addition of PMSF to a final concentration of 4 mM. Following digestion, samples were ultracentrifuged at 100,000 g for 1 h at 4 °C. The supernatant was discarded, and the pellets were resuspended by boiling in loading buffer. Samples were then analyzed by SDS-PAGE followed by immunoblotting.

**CSA for  $\alpha$ -synuclein aggregates in brain extracts.** Detergent-extracted brain homogenates were generated as described above. Twenty microliters of 2 $\times$  GdnHCl

stocks were added to an equal volume of brain extract to generate final GdnHCl concentrations of 1, 1.5, 2, 2.5, 3, 3.5 and 4 M. To generate the 0 M GdnHCl sample, 20  $\mu$ l of dH<sub>2</sub>O was added. For some CSAs on brain extract from patients with DLB and patients with AD, an extended-range CSA was performed with final GdnHCl concentrations of 1, 2, 2.5, 3, 3.5, 4, 4.5, 5, 5.5 and 6 M. Samples were then incubated at room temperature for 2 h with continuous shaking (800 r.p.m.). GdnHCl concentrations were then normalized to 0.4 M and the samples were ultracentrifuged at 100,000 g for 1 h at 4 °C using a TLA-55 rotor (Beckman). Supernatants were discarded and the pellets resuspended by boiling in loading buffer. Levels of residual  $\alpha$ -synuclein were determined by SDS-PAGE followed by immunoblotting. Densitometry was performed using ImageJ, and values were normalized to the sample with the highest intensity, which was set at 100%. GdnHCl<sub>50</sub> values were determined by nonlinear regression using the sigmoidal dose-response (variable slope) equation in GraphPad Prism, with the top and bottom values fixed at 100 and 0, respectively. GdnHCl<sub>50</sub> values were compared using two-tailed, unpaired *t*-tests or by one-way ANOVA with Tukey's multiple comparisons test. To generate denaturation curves, values for independent replicates were averaged and then normalized to the 0 M GdnHCl value (or the 1 M GdnHCl value for the extended-range CSA), which was set at 100%.

**Immunohistochemistry.** Formalin-fixed perfused mouse hemibrains were dehydrated through a graded series of ethanol using an automated tissue processor and then embedded in paraffin wax. Sagittal sections of 5  $\mu$ m thickness at the midline of the brain (−0.5–1 mm lateral) were mounted on glass slides, deparaffinized and then rehydrated using a graded series of ethanol for immunohistochemistry. Endogenous peroxidase activity was quenched by incubating the slides in 3% (v/v) H<sub>2</sub>O<sub>2</sub> prepared in methanol for 25 min, and then slides were rinsed three times (5 min each) with dH<sub>2</sub>O and once with PBS containing 0.05% (v/v) Tween-20 (PBST). Sections were blocked by incubation in 2.5% (v/v) normal horse serum for 60 min at room temperature. Immunohistochemistry was performed using rabbit monoclonal anti-PSyn EP1536Y (Abcam, ab51253; 1:320,000 dilution) or mouse monoclonal anti-p62/SQSTM1 (Abcam, ab56416; 1:10,000 dilution). The EP1536Y antibody does not cross-react with phosphorylated neurofilaments<sup>54</sup>. Sections to be stained with the p62/SQSTM1 antibody were first subjected to heat-mediated antigen retrieval in 0.1 M citrate buffer (pH 6.0). All primary antibodies were diluted in antibody diluent (Dako, S080983–2), and stainings were performed overnight at 4 °C. Following three washes with PBST (5 min each), slides were processed using ImmPress horseradish-peroxidase-labeled horse anti-rabbit or anti-mouse detection kits (Vector Laboratories, MP-7401 and MP-7402, respectively), and then washed three times (5 min each) with PBST. Slides were developed using ImmPACT 3,3'-diaminobenzidine (DAB) peroxidase substrate (Vector Laboratories, SK-4105) for 1 min, washed with tap water for 10 min, counterstained with hematoxylin and then mounted. Detection of PK-resistant  $\alpha$ -synuclein species using the antibody LB509 (Thermo Scientific, 180215; 1:500 dilution) was performed as previously described<sup>55</sup>. Brain sections were imaged using a Leica DM6000B microscope with  $\times 20$ ,  $\times 40$  or  $\times 63$  objectives in conjunction with Velocity software (v.6.3).

For semiquantitative scoring of PSyn deposition in the brains of inoculated TgM83 mice, the following scoring system was utilized: 0, no PSyn deposition; 1, mild PSyn deposition; 2, moderate PSyn deposition; 3, intense PSyn deposition. PSyn deposition was scored in the following nine different brain regions: olfactory bulb, frontal association cortex, parietal cortex, hippocampus, thalamus, hypothalamus, midbrain, cerebellar white matter and brainstem. Patterns of PSyn deposition were compared by two-way ANOVA with Sidak's multiple comparisons test. For experiments in which the olfactory bulb was missing from a few mice, a mixed-effects model with Sidak's multiple comparisons test was used. PSyn-positive astrocyte counts were conducted in the thalamus and were compared by one-way ANOVA with Tukey's multiple comparisons test. For quantification of ring-like versus LB-like PSyn deposits, counts were performed in the midbrain and then converted into percentage of total aggregates (ring-like plus LB-like). Data were compared by one-way ANOVA followed by Tukey's multiple comparisons test.

For double-labeling of PSyn and GFAP, sections were deparaffinized in xylene and rehydrated in decreasing concentrations of ethanol, followed by two washes with PBS. Epitope retrieval was performed by incubating the sections for 15 min in 0.1 M sodium citrate buffer (pH 6.0) in a steam sterilizer, followed by incubation in a blocking solution of 5% (v/v) donkey serum and 0.25% (v/v) Triton X-100 in PBS for 1 h at room temperature. The sections were then incubated with rabbit anti-PSyn EP1536Y (1:1,000 dilution) and goat anti-GFAP (Novus Biologicals, NB100–53809, 1:300 dilution) for 24 h at 4 °C. Following three washes with PBS, sections were incubated with Alexa Fluor 594-labeled donkey anti-rabbit IgG (Abcam, ab150076; 1:750 dilution) and Alexa Fluor 488-labeled donkey anti-goat IgG (Jackson ImmunoResearch Laboratories, 705–545–003; 1:1,000 dilution) for 2 h at room temperature. Nuclei were counterstained with DAPI (Sigma-Aldrich, D9542; 1:10,000 dilution). Following three washes with PBS and then 0.1 M sodium phosphate, the sections were mounted using Prolong Diamond antifade mountant (Thermo Scientific, P36961). Images were acquired using a Zeiss LSM880 scanning confocal microscope coupled to a CCD camera (Zeiss Axio Observer Z1) in

conjunction with Zen software (Carl Zeiss). Images were processed using ImageJ and Adobe Photoshop.

**Statistics and reproducibility.** All statistical analyses were performed using GraphPad Prism (v.8.2) with a significance threshold of  $P=0.05$ . Data were compared using unpaired two-tailed *t*-tests, one-way ANOVA with Tukey's multiple comparisons test or two-way ANOVA with Sidak's multiple comparisons test, as described above. Data distribution was assumed to be normal, but this was not formally tested. Data collection and analyses were not performed blinded to the conditions of the experiments. All experiments on recombinant  $\alpha$ -synuclein fibrils were performed using a minimum of three independent fibril preparations per strain. For neuropathological analysis, the brains from all inoculated mice were analyzed with the exception of the PMCA fibril second passage experiment, in which 5 out of 9 brains were examined. One brain from the third passage of the NS-fibril-derived strain was unable to be collected for analysis. For the CSAs, a minimum of three brains were analyzed per experimental condition. For nonquantitative experiments (thermolysin and PK digestion assays), a minimum of two brains were analyzed from each experimental condition, and similar results were obtained for every sample within a group.

**Reporting Summary.** Further information on research design is available in the Nature Research Reporting Summary linked to this article.

## Data availability

The data that support the findings of this study are available from the corresponding author upon reasonable request. Source data for Figs. 1 and 5–7 and Extended Data Figs. 4 and 7–10 are presented with the paper.

## References

- Chen, R. H. et al.  $\alpha$ -Synuclein membrane association is regulated by the Rab3a recycling machinery and presynaptic activity. *J. Biol. Chem.* **288**, 7438–7449 (2013).
- Lee, B. R. & Kamitani, T. Improved immunodetection of endogenous  $\alpha$ -synuclein. *PLoS One* **6**, e23939 (2011).
- Knowles, T. P. et al. An analytical solution to the kinetics of breakable filament assembly. *Science* **326**, 1533–1537 (2009).
- Rutherford, N. J., Brooks, M. & Giasson, B. I. Novel antibodies to phosphorylated  $\alpha$ -synuclein serine 129 and NFL serine 473 demonstrate the close molecular homology of these epitopes. *Acta Neuropathol. Commun.* **4**, 80 (2016).
- Ip, C. W. et al. AAV1/2-induced overexpression of A53T- $\alpha$ -synuclein in the substantia nigra results in degeneration of the nigrostriatal system with Lewy-like pathology and motor impairment: a new mouse model for Parkinson's disease. *Acta Neuropathol. Commun.* **5**, 11 (2017).

## Acknowledgements

The authors thank M. Diamond (UT Southwestern) for providing the HEK293 cells expressing YFP-tagged  $\alpha$ -synuclein(A53T) and C. Sato and P. St George-Hyslop for providing tissue from the Canadian Brain Tissue Bank. This work was supported by a new investigator award from Parkinson Canada/Pedalling for Parkinson's (to J.C.W.), grant no. MOP-136899 from the Canadian Institutes of Health Research (to J.C.W.), the Royal Society and an ERC Advanced Grant no. 669237 (to D.K.), Alberta Alzheimer's Research Program award no. APRI201700005 (to S.C.F. and H.W.), an Ontario Graduate Scholarship (to A.L.), a scholarship from the Croucher Foundation (to R.W.L.S.), a Cambridge Trust Scholarship and a Ministry of Education Technologies Incubation Scholarship, Republic of China (Taiwan) (to J.C.S.), and by a Ramon Jenkins Research Fellowship from Sidney Sussex College Cambridge (to G.M.).

## Author contributions

Designed the experiments: D.K. and J.C.W. Conducted the experiments: A.L., R.W.L.S., H.H.C.L., J.C.S., A.R.-R., S.C.F., E.S., S.M., N.P.V., R.F., M.M.M., C.S.-U. and Z.W. Analyzed and interpreted the data: A.L., G.M., P.E.F., A.T., B.T.H., H.W., M.I., D.K. and J.C.W. Wrote the manuscript: J.C.W. All authors edited and approved the manuscript.

## Competing interests

The authors declare no competing interests.

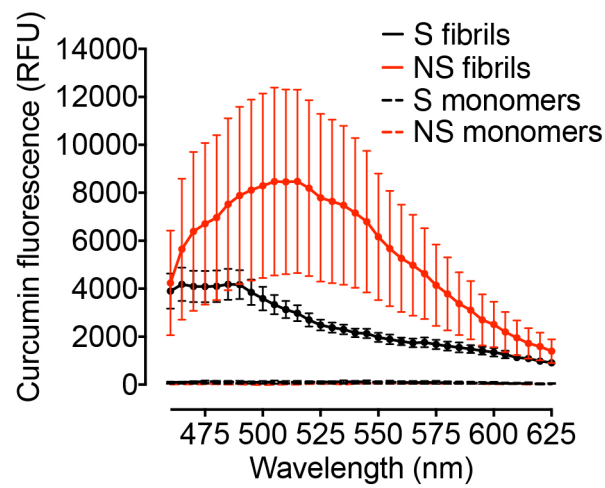
## Additional information

**Extended data** is available for this paper at <https://doi.org/10.1038/s41593-019-0541-x>.

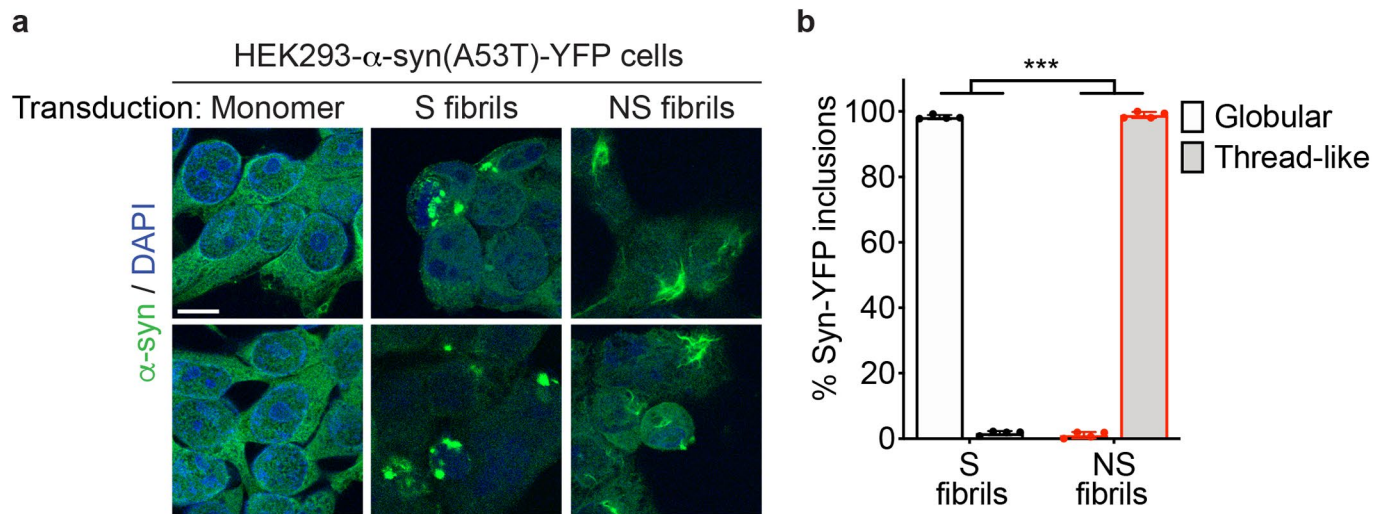
**Supplementary information** is available for this paper at <https://doi.org/10.1038/s41593-019-0541-x>.

**Correspondence and requests for materials** should be addressed to J.C.W.

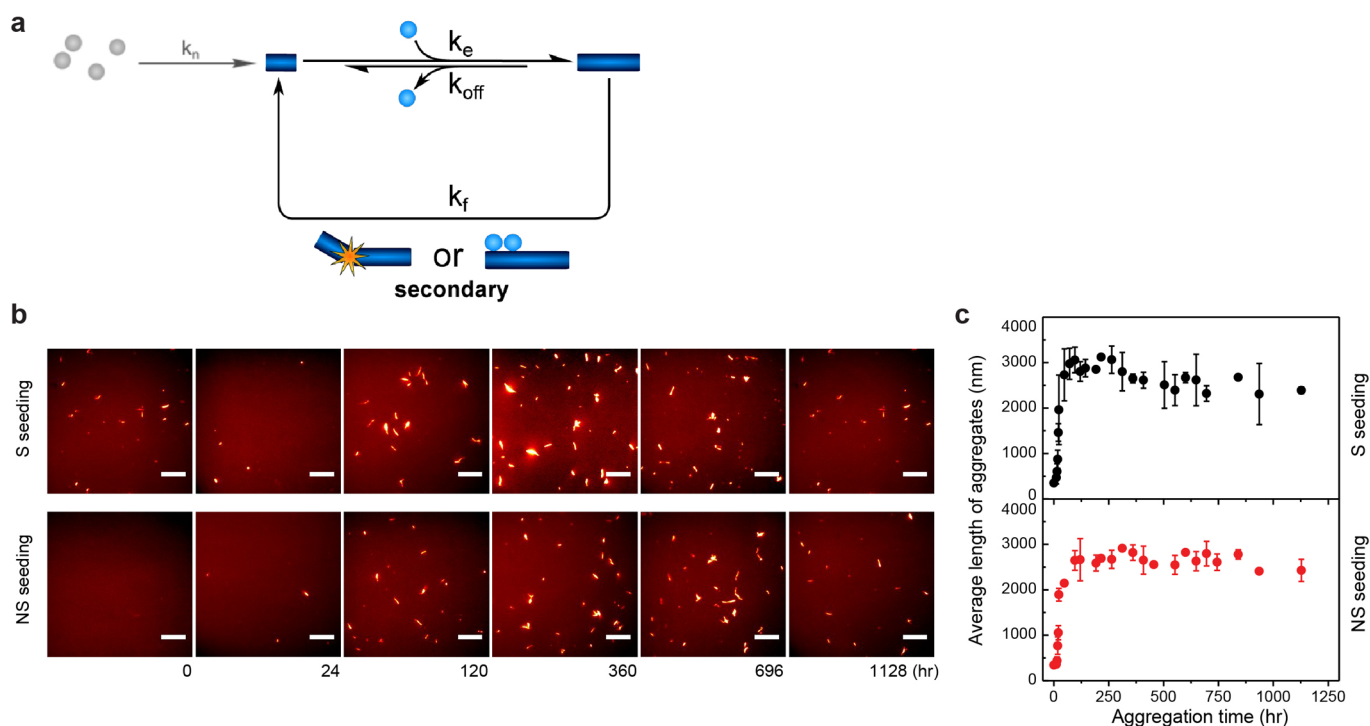
**Reprints and permissions information** is available at [www.nature.com/reprints](http://www.nature.com/reprints).



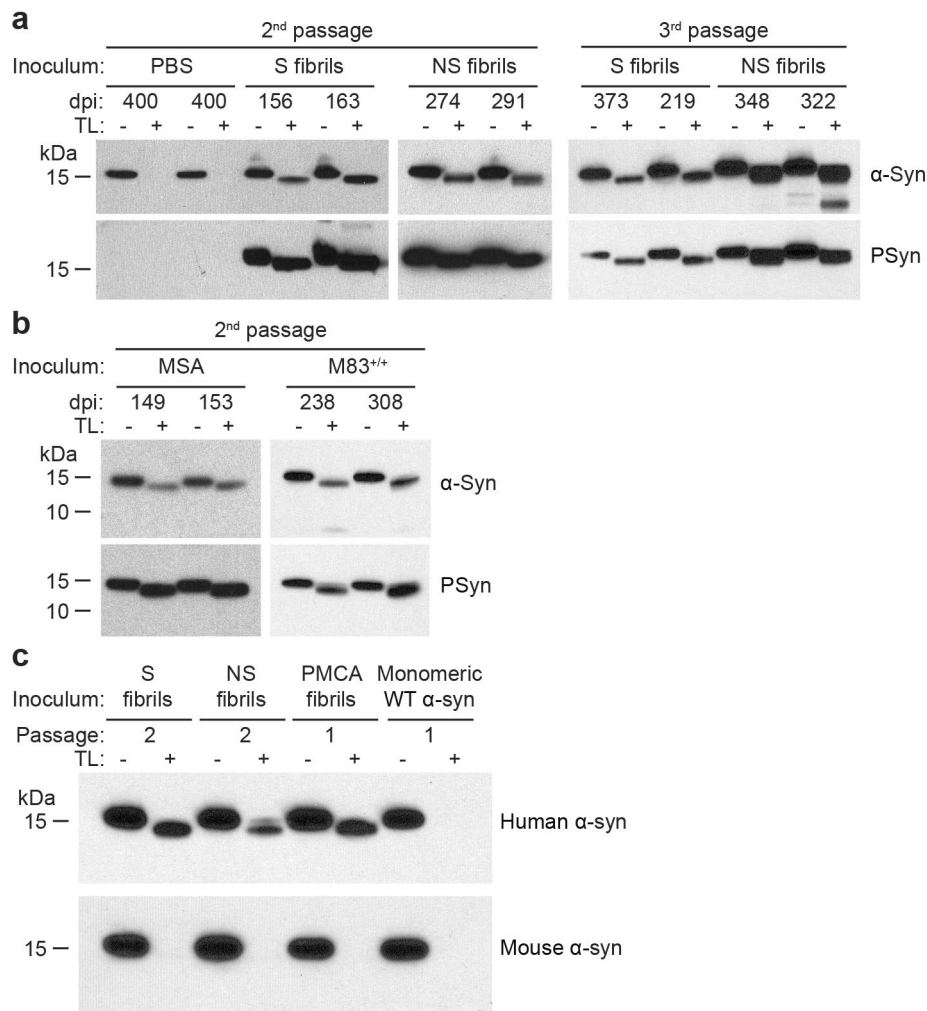
**Extended Data Fig. 1 | Non-normalized data for curcumin fluorescence spectral assay.** S fibrils, NS fibrils, or non-polymerized (monomeric) forms of recombinant  $\alpha$ -syn(A53T) were subjected to the curcumin dye-binding assay. Spectra were background-corrected but were not normalized. Only the fibrillar forms of  $\alpha$ -syn gave appreciable signal, indicating that the assay is specific for aggregates. Each data point represents the mean relative fluorescence obtained from 3 biologically independent fibril preparations  $\pm$  s.e.m.



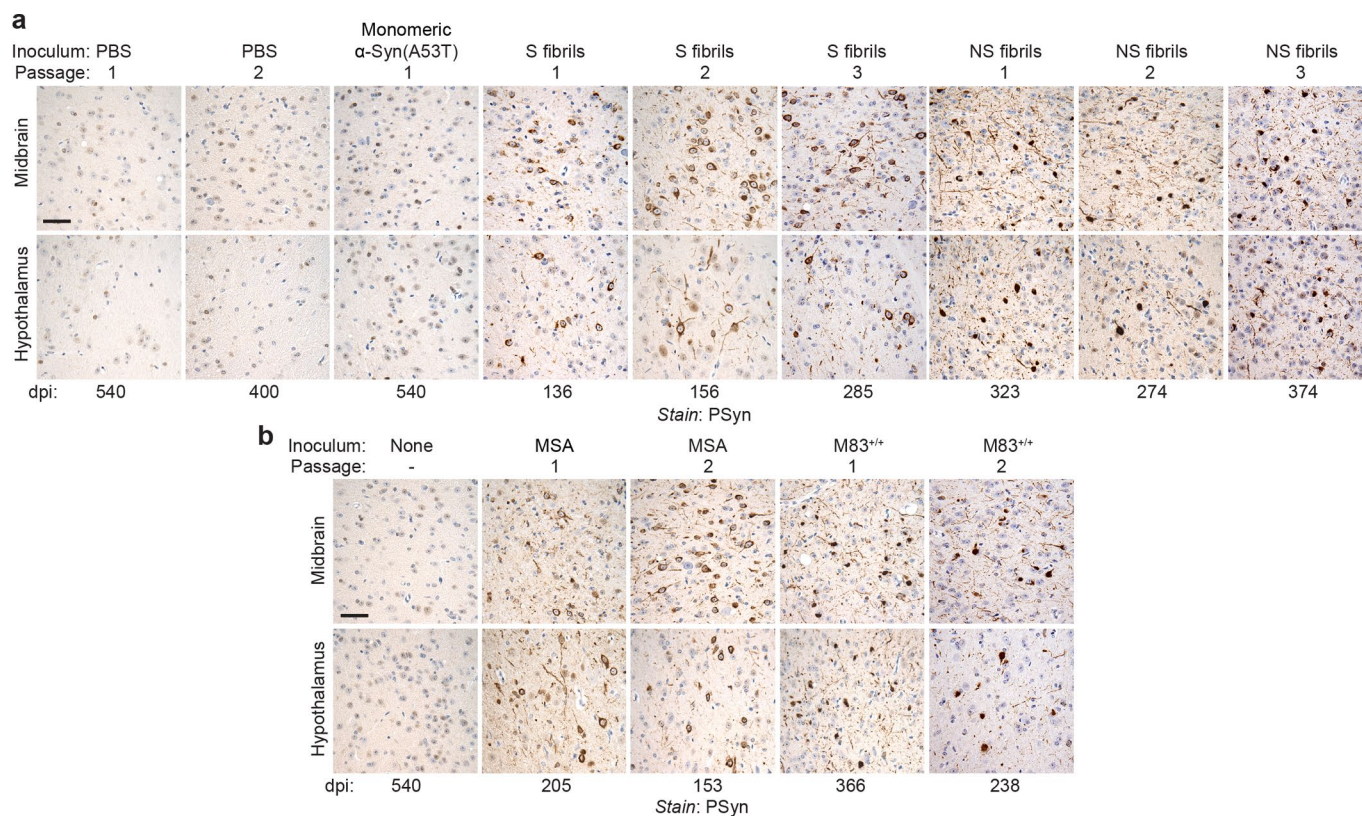
**Extended Data Fig. 2 |  $\alpha$ -Syn fibril strains produce distinct inclusions in a cultured cell bioassay. a)** HEK293 cells expressing YFP-tagged  $\alpha$ -syn(A53T) were transduced with monomeric  $\alpha$ -syn(A53T), S fibrils, or NS fibrils. Each image depicts representative cells following transduction with independent fibril preparations. Scale bar = 10  $\mu$ m (applies to all images). **b)** Cells transduced with S fibrils predominantly develop “globular” inclusions whereas cells transduced with NS fibrils predominantly develop “thread-like” inclusions ( $***P = 2.8 \times 10^{-12}$ , as determined by a two-tailed  $t$ -test). Data is mean  $\pm$  s.e.m. from 4 biologically independent transductions.



**Extended Data Fig. 3 | Single-molecule fibril seeding assay for measuring the doubling time of  $\alpha$ -syn fibril strains. **a**) Schematic of fibril assembly and fragmentation model used to determine the doubling time for  $\alpha$ -syn fibril strains. For a given concentration of monomeric  $\alpha$ -syn(A53T), the doubling time ( $t_2$ ) is determined by the rate constants for fibril elongation ( $k_e$ ) and fragmentation ( $k_f$ ). **b**) Representative ThT-stained total internal reflection fluorescence microscopy images at the indicated timepoints following seeding of monomeric  $\alpha$ -syn(A53T) with S or NS fibrils. Scale bars = 10  $\mu$ m. **c**) Single-molecule quantification of aggregate length as a function of time following seeding with S or NS fibrils. Each data point represents the mean  $\pm$  s.e.m. from 3 independent seeding reactions.**

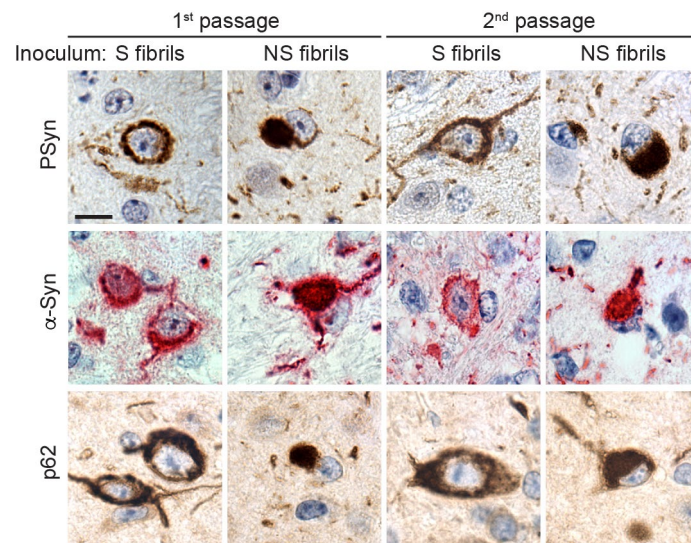


**Extended Data Fig. 4 | Additional thermolysin digestions of brain homogenates from inoculated TgM83 mice. a)** Immunoblots of detergent-insoluble  $\alpha$ -syn species in brain homogenates from the second or third passage of the S or NS fibril-derived strains in TgM83 mice, with or without digestion with thermolysin (TL). Brain homogenates from asymptomatic TgM83 mice from the second passage of PBS were used as a negative control. **b)** Immunoblots of detergent-insoluble  $\alpha$ -syn species in brain homogenates from the second passage of the MSA- or M83<sup>+/+</sup>-derived strains in TgM83 mice, with or without digestion with TL. In **a** and **b**, blots were probed with antibodies to either total  $\alpha$ -syn or PSyn. For each inoculum, results from two distinct mice are shown. dpi, days post-inoculation. **c)** Immunoblots of detergent-insoluble  $\alpha$ -syn species in brain homogenates from TgM83 mice inoculated with the indicated  $\alpha$ -syn preparations, with or without digestion with TL. Human  $\alpha$ -syn was detected with the antibody MJFR1 and mouse  $\alpha$ -syn was detected with the antibody D37A6. TL-resistant  $\alpha$ -syn species were only present in the animals injected with  $\alpha$ -syn aggregates and were only detectable with the antibody specific for human  $\alpha$ -syn.

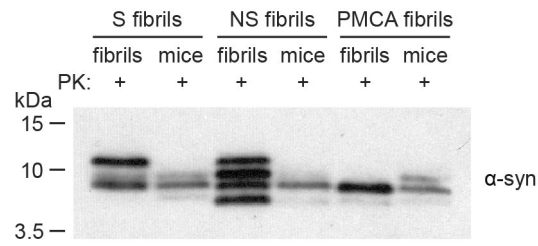


**Extended Data Fig. 5 | Phosphorylated  $\alpha$ -syn (PSyn) deposition in the midbrain and hypothalamus of TgM83 mice injected with various  $\alpha$ -syn strains.**

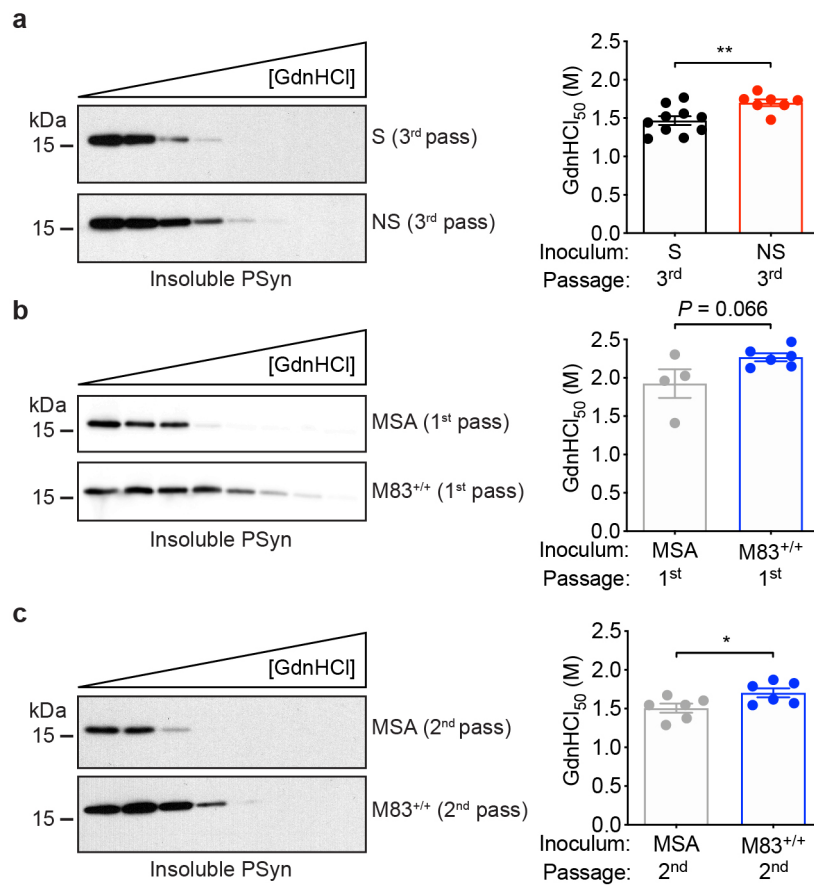
**a** Representative immunohistochemistry images for PSyn in midbrain and hypothalamus sections from asymptomatic TgM83 mice following inoculation with either PBS or monomeric  $\alpha$ -syn, or from clinically ill mice inoculated with either the S fibril- or NS fibril-derived strains (first, second, or third passage). Scale bar = 50  $\mu$ m (applies to all images). dpi, days post-inoculation. **b** Representative immunohistochemistry images for PSyn in midbrain and hypothalamus sections from asymptomatic uninoculated TgM83 mice, or from clinically ill mice inoculated with either the MSA- or M83<sup>+/+</sup>-derived strains (first or second passage). Scale bar = 50  $\mu$ m (applies to all images).



**Extended Data Fig. 6 | Additional immunohistochemical characterization of  $\alpha$ -syn inclusions in TgM83 mice inoculated with the S or NS fibril-derived strains.** Representative immunohistochemistry images for either PSyn (midbrain), PK-resistant total  $\alpha$ -syn (hypothalamus), or p62 (midbrain) in brain sections from clinically ill TgM83 mice inoculated with either the S fibril- or NS fibril-derived strains (first or second passage). Scale bar = 10  $\mu$ m (applies to all images). For each experimental group, stainings were performed on a minimum of two mice with similar results.

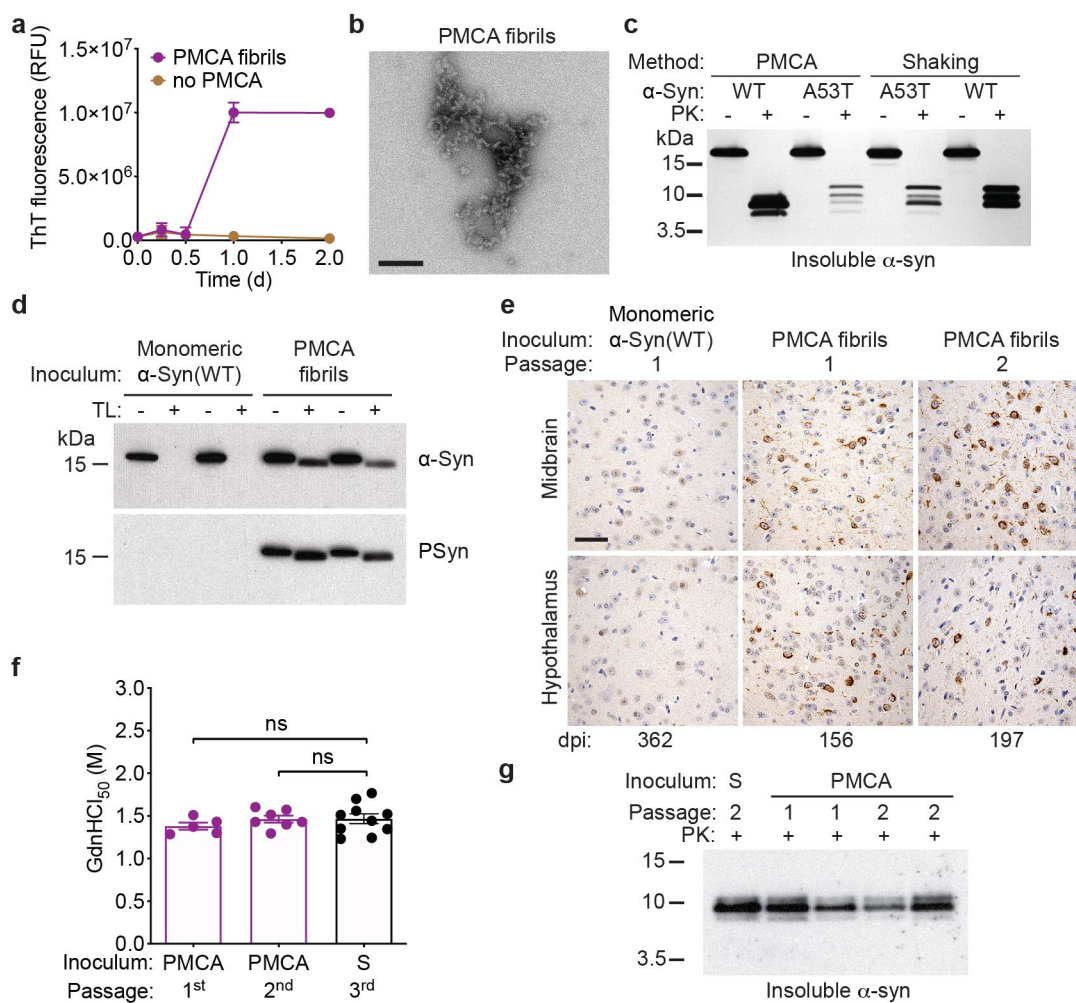


**Extended Data Fig. 7 | Comparison of PK-resistant  $\alpha$ -syn species generated from recombinant  $\alpha$ -syn fibril strains with  $\alpha$ -syn species in brain homogenates from fibril-inoculated TgM83 mice.** Immunoblot of detergent-insoluble  $\alpha$ -syn species following digestion of recombinant fibrils or brain homogenates from fibril-inoculated TgM83 mice (first passage) with PK. PK-resistant  $\alpha$ -syn was detected using the antibody Syn-1.

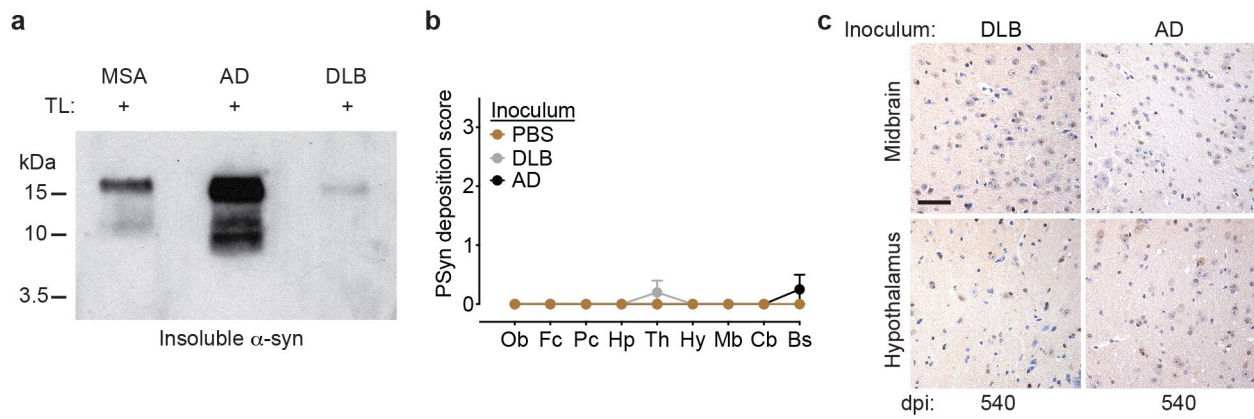


**Extended Data Fig. 8 | Additional conformational stability assay (CSA) data for  $\alpha$ -syn species in brain homogenates from inoculated TgM83 mice.**

**a** CSA for PSyn aggregates in clinically ill TgM83 mice inoculated with either the S or NS fibril-derived strains (third passage). Representative PSyn immunoblots and the resultant GdnHCl<sub>50</sub> values are shown. The PSyn aggregates in mice inoculated with the NS fibril-derived strain are significantly more stable (\*\* $P = 0.0091$ ). Data is mean  $\pm$  s.e.m (n = 10 mice for the S strain and n = 7 mice for the NS strain). **b** CSA for PSyn aggregates in clinically ill TgM83 mice inoculated with either MSA- or M83<sup>+/+</sup> brain extract (first passage). Representative PSyn immunoblots and the resultant GdnHCl<sub>50</sub> values are shown. Data is mean  $\pm$  s.e.m (n = 4 for MSA-inoculated mice, n = 6 for M83<sup>+/+</sup>-inoculated mice). **c** CSA for PSyn aggregates in clinically ill TgM83 mice inoculated with either the MSA- or M83<sup>+/+</sup>-derived strains (second passage). Representative PSyn immunoblots and the resultant GdnHCl<sub>50</sub> values are shown. The PSyn aggregates in mice inoculated with the M83<sup>+/+</sup>-derived strain are significantly more stable (\* $P = 0.038$ ). Data is mean  $\pm$  s.e.m (n = 6 for both groups of inoculated mice). All  $P$  values were obtained using a two-tailed  $t$ -test.



**Extended Data Fig. 9 | Additional characterization of PMCA-generated α-syn fibrils and PMCA fibril-inoculated TgM83 mice.** **a** Kinetics of fibril formation for PMCA fibrils in a ThT fluorescence assay. Reactions incubated at 37°C in the absence of shaking or sonication ("no PMCA") were used as a negative control. Each data point represents the mean ± s.e.m of 4 biologically independent replicates. **b** Negative stain electron micrograph of PMCA fibrils. The PMCA procedure generated fibrils that were much shorter than either the S or NS fibrils (determined using 3 biologically independent fibril preparations). Scale bar = 200 nm. **c** SDS-PAGE followed by silver staining of PK-digested α-syn fibril preparations. PMCA fibrils composed of wild-type (WT) α-syn exhibit a different banding pattern of insoluble PK-resistant α-syn species compared to S fibrils, NS fibrils, and PMCA fibrils composed of A53T-mutant α-syn. **d** Immunoblots of detergent-insoluble total α-syn and PSyn species in brain homogenates from two distinct asymptomatic monomer-inoculated mice or clinically ill PMCA fibril-inoculated mice (first passage), with or without digestion with TL. **e** Representative immunohistochemistry images for PSyn in midbrain and hypothalamus sections from asymptomatic TgM83 mice following inoculation with monomeric α-syn, or from clinically ill mice inoculated with the PMCA fibril-derived strain (first or second passage). Scale bar = 50 μm (applies to all images). **f** GdnHCl<sub>50</sub> values for PSyn aggregates in TgM83 mice inoculated with the PMCA fibril-derived strain (first or second passage) are not significantly (ns) different ( $P = 0.52$  for first passage;  $P = 0.99$  for second passage by one-way ANOVA with Tukey's multiple comparisons test) than for mice inoculated with the S fibril-derived strain (third passage). Data is mean ± s.e.m ( $n = 5$  for first passage PMCA,  $n = 7$  for second passage PMCA, and  $n = 10$  for third passage S strain). **g** Immunoblot of PK-digested and detergent-insoluble α-syn species in brain homogenates from clinically ill TgM83 mice inoculated with either the PMCA fibril-derived strain (first or second passage) or the S fibril-derived strain (second passage). Blot was probed with the Syn-1 antibody.



**Extended Data Fig. 10 | Absence of PSyn pathology in TgM83 mice inoculated with brain extract from a DLB patient or an AD patient with concomitant  $\alpha$ -syn deposition. **a**) Thermolysin digestion of brain extracts from the three human synucleinopathy samples inoculated into TgM83 mice.  $\alpha$ -Syn was detected using the antibody Syn-1. **b**) Semiquantitative PSyn deposition scoring (data are mean  $\pm$  s.e.m.) within the indicated brain regions from asymptomatic TgM83 mice at 540 days following inoculation with PBS (first passage, n = 7), DLB brain extract (n = 5), or AD brain extract (n = 4). **c**) Representative immunohistochemistry images for PSyn in midbrain and hypothalamus sections from asymptomatic TgM83 mice following inoculation with DLB or AD brain extract. Scale bar = 50  $\mu$ m (applies to all images).**

## Reporting Summary

Nature Research wishes to improve the reproducibility of the work that we publish. This form provides structure for consistency and transparency in reporting. For further information on Nature Research policies, see [Authors & Referees](#) and the [Editorial Policy Checklist](#).

### Statistics

For all statistical analyses, confirm that the following items are present in the figure legend, table legend, main text, or Methods section.

n/a Confirmed

- |                                     |                                     |  |
|-------------------------------------|-------------------------------------|--|
| <input type="checkbox"/>            | <input checked="" type="checkbox"/> | The exact sample size ( $n$ ) for each experimental group/condition, given as a discrete number and unit of measurement  |
| <input type="checkbox"/>            | <input checked="" type="checkbox"/> | A statement on whether measurements were taken from distinct samples or whether the same sample was measured repeatedly  |
| <input type="checkbox"/>            | <input checked="" type="checkbox"/> | The statistical test(s) used AND whether they are one- or two-sided<br><i>Only common tests should be described solely by name; describe more complex techniques in the Methods section.</i>   |
| <input checked="" type="checkbox"/> | <input type="checkbox"/>            | A description of all covariates tested   |
| <input type="checkbox"/>            | <input checked="" type="checkbox"/> | A description of any assumptions or corrections, such as tests of normality and adjustment for multiple comparisons  |
| <input type="checkbox"/>            | <input checked="" type="checkbox"/> | A full description of the statistical parameters including central tendency (e.g. means) or other basic estimates (e.g. regression coefficient) AND variation (e.g. standard deviation) or associated estimates of uncertainty (e.g. confidence intervals) |
| <input type="checkbox"/>            | <input checked="" type="checkbox"/> | For null hypothesis testing, the test statistic (e.g. $F$ , $t$ , $r$ ) with confidence intervals, effect sizes, degrees of freedom and $P$ value noted<br><i>Give <math>P</math> values as exact values whenever suitable.</i>                            |
| <input checked="" type="checkbox"/> | <input type="checkbox"/>            | For Bayesian analysis, information on the choice of priors and Markov chain Monte Carlo settings   |
| <input checked="" type="checkbox"/> | <input type="checkbox"/>            | For hierarchical and complex designs, identification of the appropriate level for tests and full reporting of outcomes   |
| <input checked="" type="checkbox"/> | <input type="checkbox"/>            | Estimates of effect sizes (e.g. Cohen's $d$ , Pearson's $r$ ), indicating how they were calculated   |

*Our web collection on [statistics for biologists](#) contains articles on many of the points above.*

### Software and code

Policy information about [availability of computer code](#)

Data collection

Confocal microscopy images were obtained using Zen 2.3 SP1 software (Carl Zeiss) version 14.0.5.201. Immunohistochemistry images were obtained using Volocity software (version 6.3).

Data analysis

Statistical analysis was performed using GraphPad Prism version 8.2 (for macOS). Images were processed using Image J version 1.42q and Adobe Photoshop Creative Cloud. A custom-written MATLAB script (available at Github: <https://github.com/jason82133/Particle-measurement.git>) was used for analysis of fibril doubling times.

For manuscripts utilizing custom algorithms or software that are central to the research but not yet described in published literature, software must be made available to editors/reviewers. We strongly encourage code deposition in a community repository (e.g. GitHub). See the Nature Research [guidelines for submitting code & software](#) for further information.

### Data

Policy information about [availability of data](#)

All manuscripts must include a [data availability statement](#). This statement should provide the following information, where applicable:

- Accession codes, unique identifiers, or web links for publicly available datasets
- A list of figures that have associated raw data
- A description of any restrictions on data availability

The data that support the findings of this study are available from the corresponding author upon request.

## Field-specific reporting

Please select the one below that is the best fit for your research. If you are not sure, read the appropriate sections before making your selection.

Life sciences     Behavioural & social sciences     Ecological, evolutionary & environmental sciences

For a reference copy of the document with all sections, see [nature.com/documents/nr-reporting-summary-flat.pdf](https://nature.com/documents/nr-reporting-summary-flat.pdf)

## Life sciences study design

All studies must disclose on these points even when the disclosure is negative.

|                 |  |
|-----------------|--|
| Sample size     | 4-5 mice were used for the initial passage of fibril strains to test the feasibility of our approach. For second passage, 8-10 mice were used, which is the standard number used for prion disease transmission studies (which our studies were modelled after).   |
| Data exclusions | A list of mice excluded from the study (due to intercurrent illness) is provided in Supplementary Table 4. Otherwise, no data was excluded from any of the analyses.   |
| Replication     | All in vitro studies on the fibril strains were conducted using at least 3 independent fibril preparations per strain. For neuropathological analysis, the brains from all inoculated mice were analyzed with the exception of the PMCA fibril second passage experiment, where 5 of 9 brains were examined. One brain from the third passage of NS fibrils was unable to be collected for analysis. For the conformational stability assays, a minimum of 3 mouse brains were analyzed per experimental condition. For non-quantitative experiments (thermolysin and proteinase K digestion assays), a minimum of 2 mouse brains were analyzed from each experimental condition. All replication attempts produced similar results within experimental groups. Serial passaging studies were also performed to ensure consistency of phenotype. |
| Randomization   | Weanling TgM83 mice were randomly assigned to the inoculation groups.  |
| Blinding        | Investigators scoring clinical signs of neurological illness in mice were only partially blinded to the experimental condition, but at least 2 independent people had to agree on the diagnosis for the mice to be counted as ill.   |

## Reporting for specific materials, systems and methods

We require information from authors about some types of materials, experimental systems and methods used in many studies. Here, indicate whether each material, system or method listed is relevant to your study. If you are not sure if a list item applies to your research, read the appropriate section before selecting a response.

### Materials & experimental systems

| n/a                                 | Involved in the study   |
|-------------------------------------|---|
| <input type="checkbox"/>            | <input checked="" type="checkbox"/> Antibodies                  |
| <input type="checkbox"/>            | <input checked="" type="checkbox"/> Eukaryotic cell lines       |
| <input checked="" type="checkbox"/> | <input type="checkbox"/> Palaeontology                          |
| <input type="checkbox"/>            | <input checked="" type="checkbox"/> Animals and other organisms |
| <input type="checkbox"/>            | <input checked="" type="checkbox"/> Human research participants |
| <input checked="" type="checkbox"/> | <input type="checkbox"/> Clinical data                          |

### Methods

| n/a                                 | Involved in the study                           |
|-------------------------------------|---|
| <input checked="" type="checkbox"/> | <input type="checkbox"/> ChIP-seq               |
| <input checked="" type="checkbox"/> | <input type="checkbox"/> Flow cytometry         |
| <input checked="" type="checkbox"/> | <input type="checkbox"/> MRI-based neuroimaging |

## Antibodies

### Antibodies used

The following primary antibodies were used: Anti-PSyn EP1536Y (abcam #51253; 1:320,000 dilution for immunohistochemistry, 1:1000 for fluorescent double labeling, 1:4000 for Western blotting); Anti-alpha-syn Syn-1 (aka Clone42) (BD Biosciences #610787; 1:10,000 dilution for Western blotting); Anti-alpha-syn LB509 (ThermoFisher #180215; 1:500 dilution for immunohistochemistry); anti-human  $\alpha$ -syn MJFR1 (Abcam #ab138501; 1:10,000 dilution for Western blotting); anti-murine  $\alpha$ -syn D37A6 (Cell Signaling Technology #4179; 1:10,000 dilution for Western blotting); Anti-p62/SQSTM1 (abcam #ab56416; 1:10,000 dilution for immunohistochemistry); and goat anti-GFAP (Novus Biologicals #NB100-53809; 1:300 dilution for fluorescent double labeling).

The following secondary antibodies were used: HRP-labeled goat anti-mouse and goat anti-rabbit (BioRad #172-1019 or 172-1011; 1:10,000 dilution for Western blotting; Alexa Fluor 594-labeled donkey anti-rabbit IgG (Abcam #ab150076; 1:750 dilution for fluorescent double labeling); and Alexa Fluor 488-labeled donkey anti-goat IgG (Jackson ImmunoResearch Laboratories #705-545-003; 1:1000 dilution for fluorescent double labeling).

### Validation

As per the manufacturer's website, EP1536Y reacts with human (and mouse) PSyn and is suitable for immunohistochemistry (formalin-fixed, paraffin-embedded sections) and Western blotting. Our results demonstrate that no signal is observed healthy mice, either by Western blotting (see Figure 2f) or immunohistochemistry (see Extended Data 5). Notably, EP1536Y is one of the few PSyn antibodies that does not cross react with phosphorylated neurofilament (see Rutherford et al., Acta Neuropathologica Communications, 2016).

As per the manufacturer's website, Syn-1 reacts with human (and mouse) alpha-syn and is suitable for Western blotting. When we use this antibody, a single band at the correct molecular weight for alpha-synuclein (~14 kDa) is apparent (see Figure 2f).

As per the manufacturer's website, LB509 reacts specifically with human alpha-syn and is suitable for immunohistochemistry (formalin-fixed, paraffin-embedded sections).

As per the manufacturer's website, MJFR1 reacts specifically with human alpha-syn and is suitable for Western blotting. When we use this antibody, a single band at the correct molecular weight for alpha-synuclein (~14 kDa) is apparent (see Extended Data 4).

As per the manufacturer's website, D37A6 reacts specifically with mouse (not human) alpha-syn and is suitable for Western blotting. When we use this antibody, a single band at the correct molecular weight for alpha-synuclein (~14 kDa) is apparent (see Extended Data 4).

As per the manufacturer's website, the anti-P62 antibody reacts with mouse p62/SQSTM1 and is suitable for immunohistochemistry (formalin-fixed, paraffin-embedded sections).

As per the manufacturer's website, the anti-GFAP antibody reacts with mouse GFAP and is suitable for immunohistochemistry.

## Eukaryotic cell lines

Policy information about [cell lines](#)

|  |  |
|--|--|
| Cell line source(s)  | The HEK293 cells stably expressing YFP-tagged A53T-mutant human alpha-synuclein were obtained from Marc Diamond's lab. |
| Authentication   | We did not perform additional authentication of this cell line.  |
| Mycoplasma contamination   | This cell line was not tested for mycoplasma (at least not since it arrived in my lab).                                |
| Commonly misidentified lines<br>(See <a href="#">ICLAC</a> register) | No commonly misidentified cell lines were used.  |

## Animals and other organisms

Policy information about [studies involving animals](#); [ARRIVE guidelines](#) recommended for reporting animal research

|                         |  |
|-------------------------|--|
| Laboratory animals      | Transgenic mice expressing A53T-mutant human alpha-synuclein (M83 line) were used. Both male and female mice were used in the study. Mice were inoculated at 5-6 weeks of age and then followed longitudinally up to 18 months post-inoculation. |
| Wild animals            | No wild animals were used.   |
| Field-collected samples | No field-collected samples were used.  |
| Ethics oversight        | All mouse experiments were performed in accordance with guidelines set by the Canadian Council on Animal Care under a protocol (AUP #4263.6) approved by the University Health Network Animal Care Committee.                                    |

Note that full information on the approval of the study protocol must also be provided in the manuscript.

## Human research participants

Policy information about [studies involving human research participants](#)

|                            |   |
|----------------------------|---|
| Population characteristics | A list of human synucleinopathy brain tissues utilized along with associated patient details is provided in Supplementary Table 2.  |
| Recruitment                | Samples were chosen based on neuropathological confirmation of the respective disease (MSA and DLB cases). The AD cases with concomitant pathology were selected by screening a selection of AD cases for PSyn. |
| Ethics oversight           | Brain samples were collected under protocols approved by Massachusetts General Hospital and the University of Toronto.  |

Note that full information on the approval of the study protocol must also be provided in the manuscript.